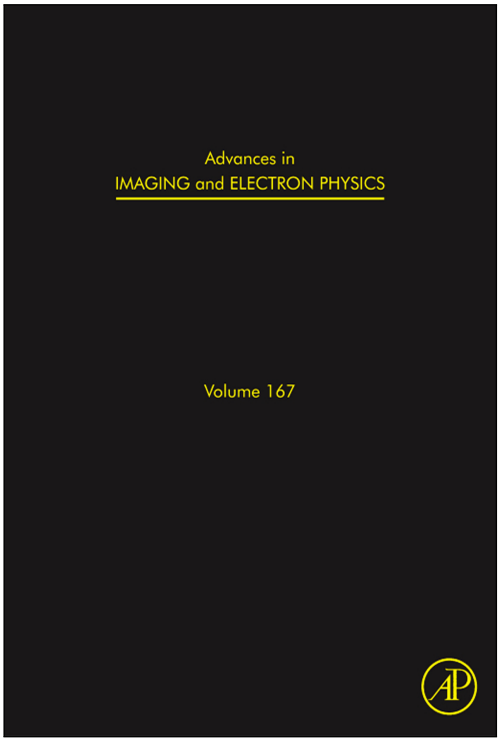

From Mohamed Ben Haj Rhouma, Mohamed Ali Khabou and Lotfi Hermi,
Shape Recognition Based on Eigenvalues of the Laplacian.
In: Peter W. Hawkes, editor, Advances in Imaging and Electron Physics, Vol 167.
San Diego: Academic Press, 2011, pp. 185–254.
ISBN: 978-0-12-385985-3

Chapter 3

Shape Recognition Based on Eigenvalues of the Laplacian

Mohamed Ben Haj Rhouma[*], **Mohamed Ali Khabou**[†], and **Lotfi Hermi**[‡]

Contents

[*] Sultan Qaboos University, Department of Mathematics and Statistics, Alkhod 123, Muscat, Oman
[†] University of West Florida, Electrical & Computer Engineering Department, Pensacola, FL 32514, USA
[‡] University of Arizona, Department of Mathematics, Tucson, AZ 85721-0089, USA

Advances in Imaging and Electron Physics, Volume 167, ISSN 1076-5670, DOI: 10.1016/B978-0-12-385985-3.00003-1.

1. INTRODUCTION

In pattern recognition, objects are usually described by numerical feature vectors that are then manipulated to create a matrix whose leading eigenvalues and eigenvectors summarize most of the important characteristics of the set of objects. In fact, eigenvalues and eigenvectors are so ubiquitous in the pattern recognition community that terms such as eigenfaces (Turk & Pentland, 1991), eigenpalms, and eigenfingers (Ribaric & Fratric, 1982) are by now standard and selfexplanatory. It is thus not surprising that recently many researchers have turned to the eigenvalues and eigenvectors of the Laplace–Beltrami operator as possible tools for shape recognition purposes (Khabou, Hermi, & Rhouma, 2007a; Khabou, Rhouma, & Hermi, 2007b, 2008; Rhouma, Khabou, & Hermi, 2009; Niethammer et al., 2007; Reuter, Wolter, & Peinecke, 2005a,b; Peinecke, Wolter, & Reuter, 2007; Reuter, Wolter, Shenton, & Niethammer, 2009b; Reuter et al., 2007, 2009a; Zuliani, Kenney, Bhagavathy, & Manjunath, 2004). Indeed, the ratios of the eigenvalues of the Dirichlet Laplacian, which correspond to the frequencies of the fixed membrane assuming the shape of the drum, satisfy the three most important criteria for shape recognition: invariance to translation, rotation, and scaling (Khabou, Hermi, & Rhouma, 2007a; Khabou, Rhouma, & Hermi, 2007b, 2008; Rosin, 2003; Torres-Mendez, Ruiz-Suarez, Sucar, & Gomez, 2000; Zhang, 2002). Eigenvalues of the Laplacian are intrinsic physical attributes describing shape.

However, there is a major difference between using the eigenvalues and eigenvectors in the classical methods such as principal component analysis (PCA) and kernel PCA and using the eigenvalues of the Laplacian for shape recognition. In classical methods, the essence of the information is stored in the eigenvectors of the leading eigenvalues, which in essence stems from the fact that an $n \times n$ matrix A can be approximated by $\tilde{A} = P^{-1}D_kP$, where D_k is a diagonal matrix whose only nonzero elements are the first k diagonal terms $D_{ii} = \lambda_i$, where $|\lambda_1| > |\lambda_2| > \cdots > |\lambda_k|$ (say, when the eigenvalues are distinct) are the dominant eigenvalues of the matrix A and P is the matrix whose columns are the eigenvectors of A. In contrast, in this chapter and in the literature mentioned above, shape is characterized using *only* the eigenvalues.

The purpose of this chapter is to provide a theoretical overview of the characteristics of the eigenvalues of four well-known linear operators and assess their usefulness as reliable tools for shape recognition. In particular, we revisit the eigenvalues of the Dirichlet and Neumann problems and

examine the recent literature on shape recognition using the Laplace operator. In addition, we will also examine the ratios of eigenvalues for the clamped plate and buckling of a clamped plate problems. To our knowledge, these are new methods that involve the bi-Laplacian, which is a fourth-order operator. Our work shows that features based on these physical eigenvalue problems are reliable tools for shape recognition.

Shape recognition techniques can be divided into numeric and non-numeric methods. By far, the most popular classification techniques are of course the numeric methods, which can also be subdivided into two groups: boundary methods and global methods. Boundary methods represent a shape by its boundary only, whereas global methods deal with all the interior points of the object. A shape recognition technique can also be classified as either information-preserving or non-preserving depending on whether full recovery of the shape being analyzed is possible from the extracted feature vectors. In this regard, all of the research in shape recognition using the eigenvalues of the Laplace–Beltrami operator belong to the class of numeric, global, and non-preserving techniques.

This chapter is structured as follows: In Section 2, we review image recognition works using Laplacian-based features and describe their most salient properties. In Section 3 we point out some theoretical results regarding the eigenvalues of the Laplacian with Dirichlet and Neumann boundary conditions with special focus on universal eigenvalue bounds. Section 4 reviews the literature for the clamped plate and buckling of a clamped plate eigenvalue problems. Both of these sections focus on the properties of the eigenvalues that are of interest to the image recognition community. In Section 5, we look in detail at the ratios of eigenvalues for each operator for simple shapes and deduce their general pattern of behavior, as well as their agreement with some established results and open conjectures. In Section 6, we explain how the numerical schemes for the various boundary conditions arise and summarize the relevant facts for these discretization procedures. Feature vectors based on these various eigenvalue problems that are both consistent and stable are described in Section 7. Artificial neural networks are central to the image classification scheme followed in this work and are thus described in Section 8. Our calculations and numerical results are described in Section 9, followed by a general conclusion.

2. RELATED WORK

In the age of digital information and imagery, shape is an integral part of every object. Accordingly, shape needs to be represented, described, matched, and retrieved effectively. Such a task is not at all evident given that shape information is found both on the boundary of and inside a domain. In fact, most shape representation and description methods can

be classified into either a contour-based method or a region-based method (Zhang & Lu, 2004; Loncarcic, 1998). *Contour-based methods* (CBMs) include simple descriptors, such as circularity, eccentricity, bending energy, convexity, circular variance, and many others (Rosin, 2003). Better-performing descriptors are extracted from one-dimensional (1D) functions such as the centroid distance, curvature, and boundary moments that are normalized to be rotation, translation, and scaling invariant (Davies, 1997). The most popular contour-based descriptor is the *Fourier descriptor* (FD), which is easy to compute and normalize (Arbter, 1989; Zahn & Roskies, 1972). Founded on the well-established Fourier theory, FDs capture both global and local features of a shape and have an acceptable noise tolerance (Arbter, 1989; Chellappa, 1984; Otterloo, 1991; Zahn & Roskies, 1972). According to the classification in Zhang (2002) and Zhang and Lu (2004), CBMs also include structural methods, such as chain code representation (Iivarinen & Visa, 1996), polygon decomposition (Groskey & Mehrotra, 1990; Groskey, Neo, & Mehrotra, 1992; Mehrotra & Gary, 1995), smooth curve decomposition (Berretti, Bimbo, & Pala, 2000), and syntactic analysis Chomsky (1957); Fu (1974). While structural methods are well suited for partial matching and occlusion problems, they are computationally costly, sensitive to noise, and difficult to implement for a general shape database (Zhang & Lu, 2004). *Region-based methods* (RBMs) take into account all points in the domain and not just those on the boundary. The famous *medial-axis transform* (MAT) Blum (1967) is the main structural method for RBM. MAT produces line segments that constitute the skeleton of a shape and that are used to represent the shape by a graph. Moments, however, constitute the primary RBMs. In fact, geometric moment invariants were among the first tools used in shape description Hu (1962) and were reported to perform well (Zhang, 2002) on a standard shape database. Algebraic moments (Niblack et al., 1993; Scassellati, Slexopoulos, & Flickner, 1994) and their generalizations to orthogonal moments such as Legendre and Zernicke moments (Kim & Kim, 2000; Teague, 1980) offer the good combination of compact features, low computational complexity, and good performance (Zhang & Lu, 2004).

As early as 1998, Shah recognized the potential of the eigenvalues of the Laplacian as a segmentation tool and hinted at its usefulness as a general pattern recognition tool (Shah, 1998). Soon after, Belkin and Niyogi (2003) used the eigenmaps of the Laplace–Beltrami operator for dimensionality and data representation and drew attention to the close ties with spectral-based clustering (Ng, Jordan, & Weiss, 2002) and already existing techniques used for image segmentation.

Since 2004, there have been several papers related to shape recognition starting with the work of Zuliani et al. (2004) who constructed a descriptor based on the eigenvalues of the Dirichlet Laplacian and showed that it has

a good retrieval accuracy for affine invariant curve and region matching. Soon after, Reuter, Wolter, and their co-authors produced a series of papers (Reuter et al., 2005a,b; Peinecke et al., 2007; Reuter et al., 2009a,b) with applications in medical imaging (Reuter et al., 2007; Niethammer et al., 2007; Reuter et al., 2009b). In their earlier work (Reuter et al., 2005a,b) they gave a comprehensive overview of the Laplace Beltrami properties, and showed that a reliable shape *DNA* or *fingerprint* for both shape matching and retrieval can be extracted. The same authors extended their work to cover both grey and color images by considering that the images are a subset of a high-dimensional Riemannian manifold (Peinecke et al., 2007). In their most recent work, Reuter et al. (2009a,b) turned to extracting shape information not from the spectrum of the Laplace operator but from the eigenfunctions. In particular, the nodal sets of the eigenfunctions and their critical points and level sets were shown to yield shape descriptors that are capable of localizing geometric properties. Exploiting the isometry invariance of eigenfunctions and using topological tools and features, they introduced a novel method for hierarchical segmentation for articulated shapes (Reuter, 2010).

In Khabou et al. (2007a,b), Khabou et al. (2008), and Rhouma et al. (2009) we examined and compared the performance of some feature vectors for Dirichlet and Neumann eigenvalues on some simple shapes using simple neural networks. We also ruled out the use of the Steklov eigenvalues as a reliable tool for shape recognition.

Recently and for the purposes of data analysis and reconstruction, (Saito, 2008) proposed a method to analyze and represent data recorded on a general d-dimensional domain of general shape by computing the eigenfunctions of a Laplacian (that is neither a Dirichlet nor a Neumann problem) defined over the domain and expanding the data into these eigenfunctions. The boundary conditions in Saito's problem emerge by requiring the Laplacian to commute with the expression of Green's function for free space. We should finally mention that for data analysis and clustering purposes, an entire school has been developed by Ronald Coifman and his students in which the Laplacian and various aspects of its spectrum play a central role (see, e.g., Coifman, Kevrekidis, Lafon, Maggioni, & Nadler, 2008; Jones, Maggioni, & Schul, 2008).

3. EIGENVALUES OF THE DIRICHLET AND NEUMANN LAPLACIANS

In this section, we provide some background information and known results about the eigenvalue problems we will use to extract feature

vectors for our shape recognition schemes. Good sources for both basic background and advanced lines for investigation include (Ashbaugh, 1999a,b; Ashbaugh & Benguria, 2007; Benguria & Linde, 2008; Courant & Hilbert, 1953; Kac, 1966; Pólya & Szegö, 1951).

3.1. The Heat and Wave Equations

At the heart of countless engineering applications are the wave and heat (sometimes called diffusion) equations

$$U_{tt} = \Delta U, \quad \text{and} \quad U_t = \Delta U$$

defined on a bounded domain $\Omega \subset \mathbb{R}^2$ and valid for $t \geq 0$, where

$$\Delta u = \frac{\partial^2 u}{\partial x^2} + \frac{\partial^2 u}{\partial y^2} \tag{3.1}$$

denotes the usual expression for the Laplacian operator.

Although we can define the problem for a higher-dimensional setting, we restrict ourselves to plane domains, since the bulk of the application presented herein falls in this category.

With either problem, there are associated classical homogeneous conditions on the boundary $\partial\Omega$ of fixed ($U|_{\partial\Omega} = 0$) or free ($\partial U/\partial n|_{\partial\Omega} := \vec{n} \cdot \nabla u|_{\partial\Omega} = 0$) type, and standard (also called Cauchy) initial conditions at $t = 0$. Here $\vec{n}$ denotes the direction of the normal to the boundary.

Separating the time and space variables in the form $U(x, y, t) = T(t)\, u(x, y)$, we are led to

$$-\lambda = \frac{T''}{T} = \frac{\Delta u}{u} \quad \text{and} \quad -\lambda = \frac{T'}{T} = \frac{\Delta u}{u}$$

depending on whether we are dealing with waves or heat dissipation. In both cases, we are led to the Helmholtz equation

$$-\Delta u = \lambda u \quad \text{in } \Omega. \tag{3.2}$$

The fixed boundary condition leads to the coupling of this equation with Dirichlet condition $u|_{\partial\Omega} = 0$, while the free case leads to its coupling with the Neumann condition $\partial u/\partial n|_{\partial\Omega} = 0$. It is well known that either problem admits a discrete spectrum $\{\lambda_n\}_{n=1}^{\infty}$ with a complete family of

corresponding orthonormal eigenfunctions $\{u_n\}_{n=1}^{\infty}$. The solution to the wave equation is then given by

$$U(x,y,t) = \sum_n \left(A_n \cos(\sqrt{\lambda_n}t + \phi_n)\right) u_n(x,y),$$

while the solution to the heat equation corresponds to

$$U(x,y,t) = \sum_n A_n e^{-\lambda_n t} u_n(x,y).$$

Here, let us immediately note that if we perform the homothety transformation $x' = \alpha\,(x - x_0)\,\cos\theta$ and $y' = \alpha(y - y_0)\,\sin\theta$, we obtain $\Delta' u = \Delta u/\alpha^2$. Therefore, the eigenvalues are scaled by $1/\alpha^2$ while they remain translation and rotation invariant. Moreover, the ratios of these eigenvalues are scale invariant. These three properties are essential for any reliable tool for shape recognition. We note that the inner product in this case is defined by

$$\langle f, g\rangle = \int\int_{\Omega} f(x,y)\overline{g}(x,y)\,dxdy.$$

With this setting the eigenvalues are known to be non-negative. Traditionally the eigenvalues of the Dirichlet Laplacian are denoted by $\lambda_1, \lambda_2, \ldots$. They are known to satisfy $0 < \lambda_1 < \lambda_2 \leq \lambda_3 \leq \lambda_k \to \infty$. The eigenvalues of the Neumann problem are usually denoted by $\mu_1, \mu_2, \ldots$. They are known to satisfy $0 = \mu_1 < \mu_2 \leq \mu_3 \leq \ldots \mu_k \to \infty$. We also point out that in the latter case, the discreteness of the spectrum is guaranteed as long as the boundary $\partial\Omega$ is not too wild. Any L^2 function f on the domain Ω can be approximated by a linear combination of a finite number of the eigenfunctions of either spectrum. In more precise terms,

$$\begin{aligned}\|f - \sum_{n=1}^{N} c_n u_n\|^2 &= \int\int_{\Omega} |f(x,y) - \sum_{n=1}^{N} c_n u_n|^2 dxdy \\ &= \int\int_{\Omega} |f(x,y)|^2 dxdy - \sum_{n=1}^{N} c_n^2 \to 0\end{aligned}$$

as $N \to \infty$, where $c_n = \langle f, u_n\rangle / \langle u_n, u_n\rangle$.

The key properties of the eigenvalues of the Dirichlet Laplacian are as follows:

(1) Domain monotonicity: If $\Omega_1 \subset \Omega_2$, then $\lambda_k(\Omega_1) \geq \lambda_k(\Omega_2)$.
(2) Eigenvalues are invariant under rigid motion (translation, rotation).
(3) For $\alpha > 0$, $\lambda_k(\alpha\,\Omega) = \dfrac{\lambda_k(\Omega)}{\alpha^2}$.
(4) Scale invariance: $\dfrac{\lambda_k(\alpha\Omega)}{\lambda_m(\alpha\Omega)} = \dfrac{\lambda_k(\Omega)}{\lambda_m(\Omega)}$.

We also note that properties 2, 3, and 4 are satisfied by the Neumann eigenvalues. There is no domain monotonicity in this case. However, the feature vectors used for our shape recognition purposes do not require such property.

3.2. The Minimax Principle

Let

$$R_1(u) = \frac{\int_\Omega |\nabla u|^2\, dxdy}{\int_\Omega u^2\, dxdy}$$

denote the Rayleigh ratio for an admissible function u defined in Ω which vanishes at the boundary. In the mechanical interpretation described in the previous section, this ratio gauges the average potential to average kinetic energy of the constrained vibration of a membrane assuming the shape of Ω, Pólya (1954). The numerator is usually called the *Dirichlet integral*.

It can be shown that the eigenvalues $\lambda_n(\Omega)$ of the Dirichlet eigenvalue problem satisfy the minimax principle

$$\lambda_n(\Omega) = \inf_M \sup_{u \in M} R_1(u), \tag{3.3}$$

where M is an n-dimensional space of $L^2(\Omega)$, the space of square integrable functions on Ω.

For a family of independent C^1 functions $g_1, g_2, \ldots, g_n$ defined on Ω and vanishing along $\partial\Omega$, form

$$u = \sum_{j=1}^{n} t_j g_j.$$

This leads to

$$R_1(u) = \frac{\sum_{i,j=1}^{n} a_{ij}\, t_i t_j}{\sum_{i,j=1}^{n} b_{ij}\, t_i t_j},$$

where

$$a_{ij} = \int_\Omega \nabla g_i \cdot \nabla g_j\, dxdy \quad \text{and} \quad b_{ij} = \int_\Omega g_i g_j\, dxdy.$$

With $A = (a_{ij})$ and $B = (b_{ij})$, form the equation

$$\left|A - \lambda B\right| = 0$$

and let the roots of this equation be denoted by $\lambda'_1 \leq \lambda'_2 \leq \cdots \leq \lambda'_n$. Poincaré proved in 1890 Forsythe and Wasow (2004); Pólya (1952b) that

$$\lambda_k \leq \lambda'_k \text{ for } k = 1, 2, \ldots, n.$$

The Rayleigh–Ritz method is the procedure of approximating the λ_k via λ'_k. Rayleigh (1894) was interested in the first eigenvalue, whereas Ritz (1909) dealt with higher eigenvalues (Waller, 1961). It is generally understood that Fischer (1905) and Courant and Hilbert (1953) independently formulated the minimax principle, and that it was the latter who fully understood its potential as a central tool in the analysis of linear problems (Courant & Hilbert, 1953; Pólya, 1954; Waller, 1961). The formulation (3.3) is favored by the finite difference community since it forms the basis of most finite difference discretization schemes. Analysts and geometers prefer the form

$$\lambda_n(\Omega) = \sup_T \inf_{u \perp T} R_1(u), \tag{3.4}$$

where T is an $n-1$-dimensional linear space and $u = 0$ on $\partial\Omega$, for $u \in T$. This formulation is the source of many of the geometric and universal inequalities described in the following sections. These two principles are equivalent, a result attributed to Peter Lax, see Pólya (1954).

3.3. Geometry and the Eigenvalues

The eigenvalues of the Dirichlet and Neumann Laplacians satisfy the Weyl asymptotic formula (Weyl, 1911)

$$\lim_{k\to\infty} \frac{\lambda_k}{k} = \lim_{k\to\infty} \frac{\mu_k}{k} = \frac{4\pi}{|\Omega|}, \tag{3.5}$$

where $|\Omega|$ denotes the area of the underlying domain Ω. These asymptotics essentially state that if Ω_1 and Ω_2 are two different domains of $\mathbb{R}^2$ with the same area, then there exists a threshold index k beyond which the ratios $\lambda_k(\Omega_2)/\lambda_k(\Omega_1)$ and $\lambda_{k+1}(\Omega)/\lambda_k(\Omega)$ get arbitrarily close to 1. This argument holds as well for the ratios $\mu_k(\Omega_2)/\mu_k(\Omega_1)$ and $\mu_{k+1}(\Omega)/\mu_k(\Omega)$. Thus, for the purposes of shape recognition, ratios of large eigenvalues do not "contain" much information. It should be noted, however, that for a given fixed index k, $\lambda_k(\Omega)/\lambda_1(\Omega)$ has geometric content and is the subject of recent optimization of shape work (Antunes & Henrot, 2011; Henrot,

2006; Henrot & Oudet, 2003; Osting, 2010; Wolf & Keller, 1994). The Weyl asymptotics satisfied by the eigenvalues are universal in the sense that there are valid for all domains. Inverting these formulas and incorporating the length of the boundary one has, according to Weyl, and as $z \to \infty$

$$N(z) \sim \frac{|\Omega|}{4\pi} z \mp \frac{|\partial\Omega|}{4\pi} \sqrt{z} + o(z^{1/2}), \tag{3.6}$$

where $N(z)$ counts the number of eigenvalues less than or equal to z and $|\partial\Omega|$ stands for the length of the boundary of Ω. Again, these asymptotics assume a smoothness condition on the boundary. The $-$ and $+$ in the second term in the asymptotics correspond to the Dirichlet and Neumann cases, respectively. In this form, one can hear both the area and length of the domain from knowing the spectrum.

Fortunately, for the case of the Dirichlet eigenvalues, ratios also satisfy a myriad of universal *domain-independent* inequalities, indicating the ratio of consecutive eigenvalues is bounded. For example, Payne, Pólya, and Weinberger (PPW; Payne et al., 1956) proved that for $k \geq 1$

$$\lambda_{k+1} - \lambda_k \leq 2\,\overline{\lambda_k}, \tag{3.7}$$

where $\overline{\lambda_k} := \frac{1}{k}\sum_{i=1}^{k} \lambda_i$ denotes the average of the first k eigenvalues. When $k = 1$, this reduces to

$$\frac{\lambda_2}{\lambda_1} \leq 3. \tag{3.8}$$

Inequality (3.7) was later improved by Hile and Protter (HP; Hile & Protter, 1980) to

$$\sum_{i=1}^{k} \frac{\lambda_i}{\lambda_{k+1} - \lambda_i} \geq \frac{k}{2}. \tag{3.9}$$

Yang (1991) obtained the inequality (see also the appendix in Cheng and Yang (2006b) where a brushed version of the bulk of Yang (1991), following the vision of Ashbaugh (2002), was published)

$$\sum_{i=1}^{k} \left(\lambda_{k+1} - \lambda_i\right)^2 \leq 2 \sum_{i=1}^{k} \lambda_i \left(\lambda_{k+1} - \lambda_i\right), \tag{3.10}$$

from which a more accessible formula, better than those of PPW and HP, ensues

$$\lambda_{k+1} \leq 3\,\overline{\lambda_k}. \tag{3.11}$$

More recent activity has led to further universal inequalities that strengthen all these previous ones. Harrell and Hermi (2008) proved that for $k \geq j \geq 1$

$$\frac{\lambda_{k+1}}{\overline{\lambda_j}} \leq 3\,\frac{k}{j}, \tag{3.12}$$

and for $k \geq \frac{4}{3}j$

$$\frac{\overline{\lambda_k}}{\overline{\lambda_j}} \leq \frac{9}{8}\,\frac{k}{j} = 1.125\,\frac{k}{j}. \tag{3.13}$$

The state of the art in this sort of universal inequalities is the statement, due to Harrell and Stubbe (1997), for $k \geq j \geq 1$

$$\frac{\overline{\lambda_k}}{\overline{\lambda_j}} \leq \frac{3}{2}\,\frac{k}{j} = 1.5\,\frac{k}{j}. \tag{3.14}$$

For individual eigenvalues, much recent activity is noteworthy. Hermi (2008) proved

$$\frac{\lambda_{k+1}}{\lambda_1} \leq 1 + 5.13265\,k. \tag{3.15}$$

Unaware of Hermi (2008), Cheng and Yang (2007) proved

$$\frac{\lambda_{k+1}}{\lambda_1} \leq 2.134\,k \quad \text{for } k \geq 3, \tag{3.16}$$

faring better than Harrell and Hermi (2008)

$$\frac{\lambda_{k+1}}{\lambda_1} \leq 2.625\,k \quad \text{for } k \geq 3. \tag{3.17}$$

Combining earlier works (Ashbaugh & Benguria, 1993b, 1994b; Ashbaugh and Benguria, 1994c) with Cheng and Yang's method (2007), Chen and Zheng (2011) recently improved these results to

$$\frac{\lambda_{k+1}}{\lambda_1} \leq 1.96194\,k \quad \text{for } k \geq 3, \tag{3.18}$$

and

$$\frac{\lambda_{k+1}}{\lambda_1} \leq 1.82417\,k \quad \text{for } k \geq 4. \tag{3.19}$$

These results were recently confirmed numerically by Osting (2010), who undertook the task of finding the *star-shaped* domain that maximizes λ_{k+1}/λ_1, for $k = 1, 12$. Assuming a representation of $\partial\Omega$ by a cosine Fourier series (thus smoothness on the boundary), Osting exhibited 13 numerically obtained domains that achieve his purposes (see Figure 3 in that paper). Note that for $k = 1, \ldots, 12$, Osting's numerical results suggest an inequality of the form

$$\frac{\lambda_{k+1}}{\lambda_1} \leq C\,k \tag{3.20}$$

with a universal constant C that does not exceed $1.269 = j_{0,1}^2/2j_{1,1}^2$, the constant corresponding to $k = 1$. Much work has been devoted to improving the bound (3.8) for λ_2/λ_1 (that is, when $k = 1$) since PPW conjectured in 1956 that

$$\frac{\lambda_2}{\lambda_1} \leq \frac{j_{0,1}^2}{j_{1,1}^2} \approx 2.539 \tag{3.21}$$

with equality if and only if Ω is a circular membrane. Here $j_{\nu,n}$ is the nth zero of the Bessel function $J_\nu(x)$. This conjecture was proved by Ashbaugh and Benguria (1991, 1992) in 1991. Melas (2003) proved the stability of the Ashbaugh and Benguria theorem under the condition that Ω is convex. For λ_3/λ_1, the optimal bound found by Osting is 3.202 (corresponding to a dumbbell) conjectured and found earlier by Levitin and Yagudin (2003). This optimal bound has been disproved numerically by Trefethen and Betcke (2006), who exhibited a "two-disk domain" with two cusps for which λ_3/λ_1 falls short by 0.35% of the Levitin–Yagudin value. However, Levitin and Yagudin (2003) and Trefethen and Betcke (2006) duly note that the optimal domain satisfies the condition $\lambda_3 = \lambda_4$. "Feasibility regions" for all possible values of λ_3/λ_1 vs. λ_2/λ_1 have been displayed and discussed by various authors (see Ashbaugh, 1999b; Ashbaugh and Benguria, 1994b,c; Levitin and Yagudin, 2003; Chen and Zheng, 2011). The paper by Chen and Zheng (2011) has the best bounds to date:

$$3.1818 \leq \sup_{\Omega} \frac{\lambda_3}{\lambda_1} \leq 3.73785. \tag{3.22}$$

The lower bound corresponds to the fraction 35/11 obtained for the $\sqrt{3} \times \sqrt{8}$ rectangle.

The low eigenvalues of the Dirichlet Laplacian also contain information that is shape specific. For example, the first eigenvalues λ_1, called the *dominant mode*, are known to contain information about the geometry. We

have, for example, the Rayleigh-Faber-Krahn inequality

$$\lambda_1 \geq \frac{\pi j_{0,1}^2}{|\Omega|},$$

where $j_{0,1} = 2.4048\ldots$ is the first zero of the Bessel function of first kind $J_0(x)$. This is an isoperimetric inequality. Equality holds when the domain Ω is a disk. This inequality is stable when Ω is convex in the following sense: If the eigenvalue $\lambda_1(\Omega)$ is close to that of the disk of the same area, then the domain Ω is trapped between two disks whose areas are close to Ω. This result was proved by Melas (2003). A new result that strays away from the convexity condition and gauges the stability of the Faber–Krahn inequality in terms of a measure of the asymmetry of Ω has been recently proved by Fusco, Maggi, & Pratelli (2009). Also for convex planar domains, we have the inequalities of Makai (1962) and Pólya (1960) (see also Antunes and Freitas, 2006; Antunes & Henrot, 2011; Henrot, 2006):

$$\frac{\pi^2|\partial\Omega|^2}{16|\Omega|^2} \leq \lambda_1 \leq \frac{\pi^2|\partial\Omega|^2}{4|\Omega|^2}.$$

A well-known conjecture of Pólya and Szegö (1951) states that of all n-polygons with the same area, the regular n-polygon is the one with the smallest first eigenvalue. This has been proved by Pólya for $n = 3, 4$ but is still an open problem. More recently, Antunes and Freitas (2006) used a mesh-free numerical approach to establish several conjectures regarding the dependence of the dominant mode on the perimeter and the area.

In addition, one can prove inequalities relating the eigenvalues of the Dirichlet Laplacian with the moments $I_\alpha = \int_\Omega r^\alpha dr$. For example, Ashbaugh and Hermi (2008) proved

$$(\lambda_{m+1} - \lambda_m)\left(\sum_{i=1}^{m}\frac{1}{\lambda_i^2}\right) \leq C_{p,q}\left(I_{2p}^{(q-1)/q}\sum_{i=1}^{m}\frac{1}{\lambda_i^{2-1/q}} + 2pI_{2p-2}^{(q-1)/q}\sum_{i=1}^{m}\frac{1}{\lambda_i^{(q-1)/q}}\right)$$

for any integers $p \geq 1$ and $q \geq 1$ and where $C_{p,q}$ is a universal constant depending on p and q alone. It is worth mentioning here that invariants based on moments have been used previously as tools for shape recognition (see, e.g., Flussera & Suka, 1993; Khotanzad & Hong, 1990; Reeves, Prokop, Andrews, & Kuhl, 1988).

A minimax principle similar to the Dirichlet problem (in both forms) holds in this case for C^1 functions u with support on Ω for which $\int_\Omega u\,dxdy = 0$. Examples of universal eigenvalue bounds for the Neumann case include

$$\mu_k(\Omega) \leq \lambda_k(\Omega),$$

which follows immediately from the minimax principle. Kornhauser and Stakgold (1952) (see also Pólya, 1952b) were the first to prove the statement that $\mu_2 \leq \lambda_1$, a result which was generalized by Payne (1962) for Ω convex and smooth

$$\mu_{k+1}(\Omega) \leq \lambda_k(\Omega). \tag{3.23}$$

Payne conjectured, Payne (1967), that this result was true in its full generality was settled in 1991 by Friedlander. There are no known universal ratio bounds involving the Neumann eigenvalues, however, based on observations, Ashbaugh and Benguria (1993b) conjectured (see also Ashbaugh, 1999b) the sharp bound

$$\frac{\mu_3(\Omega)}{\mu_2(\Omega)} < 4 \tag{3.24}$$

when Ω is convex. This ratio approaches the value 4 when Ω tends to an infinite strip. This question has been recently treated numerically by Antunes and Henrot (2011). There are many inequalities relating the geometry of Ω to the Neumann spectrum. The oldest result of this type is the Szegö–Weinberger inequality (see Szegö, 1954; Weinberger, 1956)

$$\mu_2 \leq \frac{p^2\pi}{|\Omega|} \tag{3.25}$$

with equality when Ω is a disk. Here $p = 1.8412$ is the smallest positive zero of $J_1'(x)$. Kröger (1992) also proved that

$$\sum_{j=1}^{k} \mu_j \leq \frac{1}{2}\frac{4\pi k^2}{|\Omega|}, \tag{3.26}$$

which in other words states that the Weyl asymptotic, on average, is an upper bound for the Neumann eigenvalues. We note the recent paper (Girouard & Polterovich, 2010) for new results relating the spectrum of the Neumann problem and the geometry of the underlying domain. In what follows, when we discuss Neumann eigenvalues, we will simply dismiss $\mu_1 = 0$ to avoid dividing by zero, so the first ratio would simply be μ_3/μ_2.

4. THE CLAMPED PLATE AND BUCKLING OF A CLAMPED PLATE PROBLEMS

As told by various authors (Stoker, 1942; Ullmann, 2007; Waller, 1961), the initial mathematical formulation of vibration of thin plates goes back

to the German physicist Ernest Chladni (1786) who, as one of early "science globetrotters," first popularized the subject through his experiments stroking violin bows over metal plates covered with sand. Explaining the patterns that resulted from this mechanical excitation of plates became a fertile ground for good mathematics for the next 20 years with contributions by James Bernoulli; Sophie Germain, who in 1815 won the prize set by the French Academy at the behest of Napoleon Bonaparte six years before; and Lagrange, who corrected Germain's theory and derived the equations of vibration of plates as we know them today.

The vibration of a clamped plate assuming the shape of $\Omega \subset \mathbb{R}^2$ is governed by the equation

$$\Delta^2 u = \Gamma u \quad \text{in } \Omega \quad u = \frac{\partial u}{\partial n} = 0 \text{ on } \partial\Omega, \tag{4.1}$$

where Δ^2 is the biharmonic operator given by

$$\Delta^2 u = \frac{\partial^4 u}{\partial x^4} + 2\frac{\partial^4 v}{\partial x^2 \partial y^2} + \frac{\partial^4 u}{\partial y^4}$$

plays the role of the Laplacian in wave equation described in Section 1. The boundary conditions in this case are usually called "clamped" (thus the "clamped plate problem") or Kirchoff conditions, after the Russian mathematician who made significant contributions to the subject in 1850s Stoker (1942).

The problem at hand is a fourth order eigenvalue problem. As in the case of the Dirichlet and Neumann problems, this equation exhibits a discrete spectrum, denoted by $0 < \Gamma_1 \leq \Gamma_2 \leq \cdots$. These eigenvalues are invariant under translation or rotation of the domain Ω. Moreover, for $\alpha > 0$ and for $\alpha\,\Omega$ denoting the scaling of the domain Ω by α, one has

(1) $\Gamma_k(\alpha\Omega) = \dfrac{\Gamma_k(\Omega)}{\alpha^4}$, and

(2) $\dfrac{\Gamma_k(\alpha\Omega)}{\Gamma_m(\alpha\Omega)} = \dfrac{\Gamma_k(\Omega)}{\Gamma_m(\Omega)}$.

These properties make the ratios of eigenvalues in this case suitable to construct feature vectors for pattern recognition purposes.

The eigenvalues of the clamped plate satisfy a Weyl asymptotic formula which states that they grow like k^2 when k is large. In fact, as $k \to \infty$,

$$\Gamma_k \approx \frac{16\pi^2 k^2}{|\Omega|^2}, \tag{4.2}$$

where $|\Omega|$ denotes the area of Ω. They also satisfy a host of *inequalities*. For example, one has the Li–Yau-type inequality (see, e.g.,

Harrell & Hermi (2008); Harrell et al. (2008); Hermi (2008))

$$\Gamma_k \geq \frac{16\pi^2 k^2}{3|\Omega|^2}. \tag{4.3}$$

The Rayleigh function characterizing these eigenvalues is given by

$$R_2(u) = \frac{\int_\Omega (\Delta u)^2}{\int_\Omega u^2}. \tag{4.4}$$

In this case, the minimax principle takes the form

$$\Gamma_k(\Omega) = \inf_M \sup_{u \in M} R_2(u), \tag{4.5}$$

where M is an n-dimensional space of $L^2(\Omega)$, the space of square integrable functions with support on Ω that satisfy the clamped boundary conditions. For an admissible function in this Rayleigh–Ritz principle, we note that the Cauchy–Schwarz inequality leads to

$$\left(\int_\Omega |\nabla u|^2\right)^2 = \left(-\int_\Omega u\Delta u\right)^2 \leq \left(\int_\Omega u^2\right)\left(\int_\Omega (\Delta u)^2\right). \tag{4.6}$$

Therefore

$$\left(\frac{\int_\Omega |\nabla u|^2}{\int_\Omega u^2}\right)^2 \leq \frac{\int_\Omega (\Delta u)^2}{\int_\Omega u^2},$$

or

$$\lambda_k^2(\Omega) \leq \Gamma_k(\Omega). \tag{4.7}$$

This argument goes back to Szegö (1950). It can also be found in later work of Payne and Weinberger (1958) and the more recent work of Ashbaugh et al. (1997); Ashbaugh and Laugesen (1996).

We also have a gamut of *universal inequalities*, paralleling the case of the Dirichlet eigenvalues, relating the eigenvalue of clamped plate to each other, without reference to the underlying domain. The earliest of such inequalities was proved by Payne et al. (1956):

$$\Gamma_{k+1} - \Gamma_k \leq \frac{8}{k}\sum_{j=1}^{k} \Gamma_j, \tag{4.8}$$

from which it follows (when $k = 1$) that

$$\frac{\Gamma_2}{\Gamma_1} \leq 9. \tag{4.9}$$

Ashbaugh (1999b) observed in the excellent review of these problems that (4.8) follows from the stronger inequality

$$\Gamma_{k+1} - \Gamma_k \leq \frac{8}{k^2} \left(\sum_{j=1}^{k} \sqrt{\Gamma_j} \right)^2, \tag{4.10}$$

which reduces also (4.9) when $k = 1$. Hile and Yeh (1984) proved the inequality

$$\frac{k^{3/2}}{8} \leq \left(\sum_{j=1}^{k} \frac{\Gamma_j^{1/2}}{\Gamma_{k+1} - \Gamma_j} \right) \left(\sum_{j=1}^{k} \Gamma_j \right). \tag{4.11}$$

A stronger result in this vein was shown independently by Hook and Chen & Qian in 1990 (see Ashbaugh (1999b))

$$\frac{k^2}{8} \leq \left(\sum_{j=1}^{k} \frac{\sqrt{\Gamma_j}}{\Gamma_{k+1} - \Gamma_j} \right) \left(\sum_{j=1}^{k} \sqrt{\Gamma_j} \right). \tag{4.12}$$

There is still activity in this field with the recent results of Cheng and Yang (2006a):

$$\Gamma_{k+1} - \frac{1}{k} \sum_{j=1}^{k} \Gamma_j \leq \sqrt{8} \frac{1}{k} \sum_{j=1}^{k} \sqrt{\Gamma_j \left(\Gamma_{k+1} - \Gamma_j \right)}, \tag{4.13}$$

and Wang and Xia (2010):

$$\sum_{j=1}^{k} \left(\Gamma_{k+1} - \Gamma_j \right)^2 \leq \sqrt{8} \left(\sum_{j=1}^{k} \left(\Gamma_{k+1} - \Gamma_j \right)^2 \sqrt{\Gamma_j} \right)^{1/2} \left(\sum_{j=1}^{k} \left(\Gamma_{k+1} - \Gamma_j \right) \sqrt{\Gamma_j} \right)^{1/2}. \tag{4.14}$$

Ashbaugh (1999a) conjectured that one might be able to improve (4.9) to

$$\frac{\Gamma_2(\Omega)}{\Gamma_1(\Omega)} \leq \frac{\Gamma_2(\text{Disk})}{\Gamma_1(\text{Disk})} \approx 4.3311. \tag{4.15}$$

The buckling of a clamped plate problem (buckling problem) is described by the eigenvalue problem

$$\Delta^2 u = -\Lambda\, \Delta u \quad \text{in } \Omega \text{ subject to } u = \frac{\partial u}{\partial \nu} = 0 \text{ on } \partial\Omega. \tag{4.16}$$

This problem admits a discrete spectrum $0 < \Lambda_1 \leq \Lambda_2 \leq \cdots \to \infty$. The critical buckling load of a clamped plate subject to a uniform compressive force around its boundary is the first eigenvalue Λ_1 of this problem. This is the quantity of most interest to structural engineers. The Rayleigh function characterizing these eigenvalues is then given by

$$R_3(u) = \frac{\int_\Omega (\Delta u)^2}{\int_\Omega |\nabla u|^2}. \tag{4.17}$$

In this case, the minimax principle takes the form

$$\Lambda_k(\Omega) = \inf_M \sup_{u \in M} R_3(u). \tag{4.18}$$

For an admissible function in this Rayleigh–Ritz principle, we note also that the Cauchy–Schwarz inequality (4.6) leads to

$$\frac{\int_\Omega |\nabla u|^2}{\int_\Omega u^2} \leq \frac{\int_\Omega (\Delta u)^2}{\int_\Omega |\nabla u|^2}$$

or

$$\lambda_k(\Omega) \leq \Lambda_k(\Omega). \tag{4.19}$$

Szegö proved in 1950 that

$$\Gamma_1 \geq \lambda_1\, \Lambda_1.$$

This follows from the Cauchy–Schwarz inequality and the Rayleigh–Ritz principles for these problems. The paper by Ashbaugh (2004) offers a good review of the main properties of the buckling problem. The first systematic study of this problem goes back to a 1937 mémoire by Weinstein (1937, 1966) (see Payne, 1967), who conjectured that the second eigenvalue of the Dirichlet eigenvalue is a low bound for the critical buckling load

$$\lambda_2 \leq \Lambda_1$$

with equality if Ω is a circular plate. This isoperimetric inequality was proved by Payne in 1955 (see also Payne, 1991, 1967). It is to be noted that when Ω is convex, Payne (1960/1961) also showed the counterpart inequality

$$\Lambda_1 \leq 4\lambda_1$$

with equality for the infinite strip (that is an elongated rectangle). Also when Ω is convex, Payne (1960/1961) showed that

$$\Gamma_1 \leq \frac{16}{3}\lambda_1^2$$

with equality again for the infinite strip. One should note the well-known result that states that

$$\Gamma_1 \leq \Lambda_1^2$$

follows immediately from the minimax principles for both.

The Weyl (1911) asymptotics

$$\Lambda_k \approx \frac{4\pi k}{|\Omega|} \tag{4.20}$$

for the buckling problem was proved only recently Ashbaugh et al. (2010). For a flavor of bounds in the spirit of Faber–Krahn, we note that Pólya and Szegö (1951) conjectured the isoperimetric inequality

$$\Lambda_1(\Omega) \geq \Lambda_1(\Omega^*) = \frac{\pi j_{1,1}^2}{|\Omega|}, \tag{4.21}$$

where Ω^* is the disk with the same area as Ω, and $j_{1,1} \approx 3.83171$. Bramble and Payne (1963) showed the weaker inequality

$$\Lambda_1(\Omega) > \frac{2\pi j_{0,1}^2}{|\Omega|} = c_2\, \Lambda_1(\Omega^*) \tag{4.22}$$

with $c_2 \approx 0.787794$ (see also Ashbaugh and Laugesen, 1996; Ashbaugh et al., 1997 for higher-dimensional versions).

The buckling eigenvalues are intrinsic physical properties of the underlying domain Ω and are thus invariant under translation and rotation. They also satisfy the following scaling properties:

$$\Lambda_k(\alpha\Omega) = \frac{\Lambda_k(\Omega)}{\alpha^2}, \quad \text{and}$$
$$\frac{\Lambda_k(\alpha\Omega)}{\Lambda_m(\alpha\Omega)} = \frac{\Lambda_k(\Omega)}{\Lambda_m(\Omega)}.$$

The buckling eigenvalues also satisfy universal eigenvalue inequalities similar to those described earlier. PPW Payne et al. (1956) proved in their celebrated paper that

$$\frac{\Lambda_2}{\Lambda_1} \leq 3.$$

Hile and Yeh (1984) improved this result to

$$\frac{\Lambda_2}{\Lambda_1} \leq 2.5. \tag{4.23}$$

For higher eigenvalues, Ashbaugh (1999a) (see also Ashbaugh, 2004) proved

$$\frac{\Lambda_2 + \Lambda_3}{\Lambda_1} \leq 6$$

and a host of other stronger inequalities gauging Λ_3/Λ_1 in terms of Λ_2/Λ_1. In 2006, Cheng and Yang were able to prove that

$$\sum_{j=1}^{k} \left(\Lambda_{k+1} - \Lambda_j\right)^2 \leq 4 \sum_{j=1}^{k} \Lambda_j \left(\Lambda_{k+1} - \Lambda_j\right).$$

They also conjecture that one can improve this inequality to

$$\sum_{j=1}^{k} \left(\Lambda_{k+1} - \Lambda_j\right)^2 \leq 2 \sum_{j=1}^{k} \Lambda_j \left(\Lambda_{k+1} - \Lambda_j\right)$$

an inequality that would be sharp in the sense of Weyl's asymptotic formula (4.20). One should finally note the conjecture suggested by Ashbaugh (1999a) that

$$\frac{\Lambda_2(\Omega)}{\Lambda_1(\Omega)} \leq \frac{\Lambda_2(\text{Disk})}{\Lambda_1(\text{Disk})} \approx 1.83079. \tag{4.24}$$

5. LESSONS FROM SIMPLE SHAPES

In 1992, Gordon, Webb, & Wolpert (1992) gave the first example of two isospectral shapes in the plane (i.e., different shapes with the same eigenvalues of the Dirichlet Laplacian). The two shapes, commonly known as *Bilby* and *Hawk*, provided an explicit two-dimensional negative answer to

the question posed by Bochner and Kac in the much-quoted paper, "Can One Hear the Shape of a Drum?" Kac (1966). Soon after Bilby and Hawk, many other isospectral domains were invented by mathematicians (Buser, Conway, Doyle, & Semmler, 1994)[1]. The isospectrality of Bilby and Hawk was tested experimentally by physicists (Sridhar & Kudrolli, 1994) and computed numerically using various techniques, including the 5-point scheme described below (see Betcke & Trefethen, 2005; Driscoll, 1997; Okada, Shudo, Tasaki, & Harayama, 2005; Wu, Sprung, & Martorell, 1995). Two other isospectral domains, affectionately called *Aye-Aye* and *Beluga*, are the subject of a recent experiment in nanotechnology Moon et al. (2008). Unfortunately, these isospectral examples say that, in general, the eigenvalues do not give a unique characterization of the shape. However, this setback can be quickly overcome by another set of evidence—some experimental and some theoretical—that indicates that these isospectral domains are the exception rather than the rule. For example, new positive theoretical results by Zelditch (2000) prove that for domains that possess the symmetry of an ellipse and satisfy some generic conditions on the boundary, the spectrum of the Dirichlet Laplacian uniquely determines the shape. Later, Zelditch (2004, 2009) improved this result to real analytic plane domains with only one symmetry.

In this section, we design a few simple experiments to match theoretical results described earlier with the finite difference code developed for the various implementations of the eigenvalues at hand, and to gauge some of the separability properties with a few features. The shapes considered in these simple experiments are rectangles, diamonds, ellipses, and triangles (Figure 1). The case of a disk has been thoroughly discussed in earlier sections, so here we briefly discuss rectangles. For a rectangle

$$\square = \{0 < x < L, 0 < y < W\},$$

the eigenvalues of the Dirichlet Laplacian are given by

$$\lambda_{\ell m}(\square) = \pi^2 \left(\frac{\ell^2}{L^2} + \frac{m^2}{W^2} \right),$$

where ℓ and m are positive integers. It is clear that its aspect ratio $R = L/W$, which is invariant to scaling, can be deduced from the first ratio (see also Ashbaugh and Benguria, 1994b,c; Levitin and Yagudin, 2003)

$$\frac{\lambda_2(\square)}{\lambda_1(\square)} = \frac{R^2 + 4}{R^2 + 1} \quad \text{for} \quad R \geq 1, \tag{5.1}$$

[1] A gallery of such domains is available online; see http://www.geom.uiuc.edu/docs/research/drums/cover/cover.html

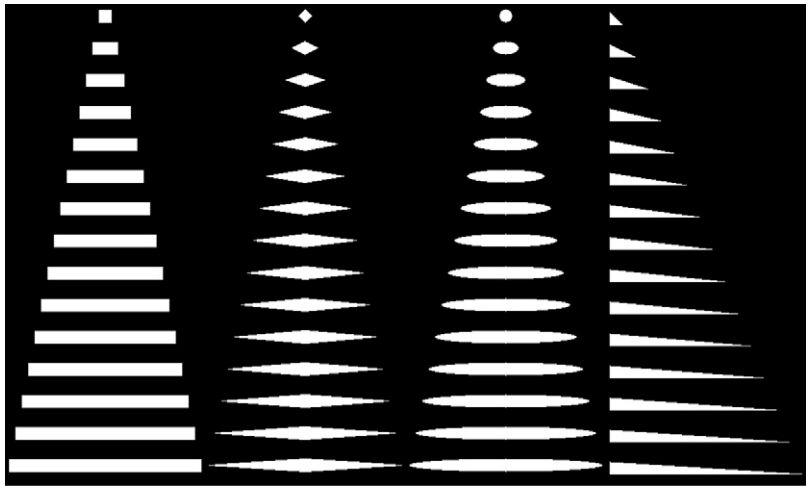

FIGURE 1 Different basic shapes of varying aspect ratios ranging from 1:1 to 15:1.

that is—one can hear the aspect ratio of a rectangle. It is also clear from Eq. (5.1) that when $R \to \infty$, the value of λ_2/λ_1, and more generally $\frac{\lambda_m(\square)}{\lambda_n(\square)}$, tend to constants and thus fails to identify much the aspect ratio. This is exhibited in the asymptotic behavior shown in Figures 2 and 3 when curves level off as the aspect ratio diverges. In this case, the rectangle reduces to an infinite thin strip, so essentially a 1D structure for which the eigenvalues cluster. This phenomenon is not unique to rectangles. In the figures just described, we have generated graphs for λ_1/λ_2 for the four problems at hand and the four basic shapes. One of the graphs in Figure 2a corresponds Eq. (5.1) for rectangles. All the curves, regard-less of the operator or the shape, level off as $R \to \infty$. Figure 2b, which deals with the Neumann case, shows that λ_1/λ_2 tends to $1/4$ from above as the aspect ratio tends to ∞ corresponding to infinite strips as conjectured by Ashbaugh and Benguria in (3.24). When the aspect ratio is equal to 1, all the graphs "cluster" near a specific value for λ_1/λ_2. In the case of the Dirichlet, clamped, and buckling cases, the circle provides the lowest possible value (when $R = 1$), and the more symmetric the body, the lower is the ratio (so among all rectangles and diamonds, the square provides a minimal value for the ratio), and among all ellipses, the circle is the minimizer. For these cases, the membranes have fourfold symmetry, an aspect ratio equal to 1, and $\mu_2 = \mu_3$. The graphs confirm this for the basic shapes considered. The middle range of aspect ratios should be used to guarantee the separability of basic shapes.

Interestingly, for simple shapes with large aspect ratios, the ratio of the first two eigenvalues for Dirichlet, Neumann, and clamped plate cases

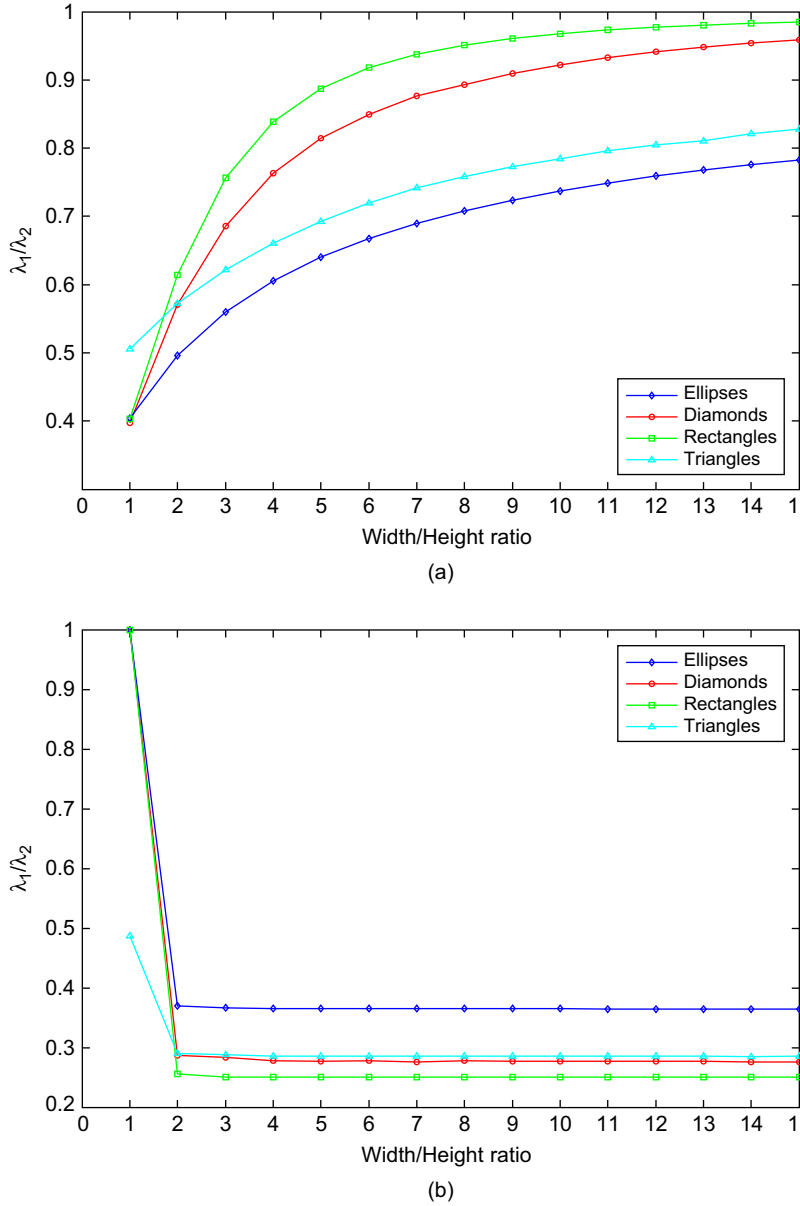

FIGURE 2 λ_1/λ_2 for basic shapes of varying aspect ratios: (a) Dirichlet; (b) Neumann.

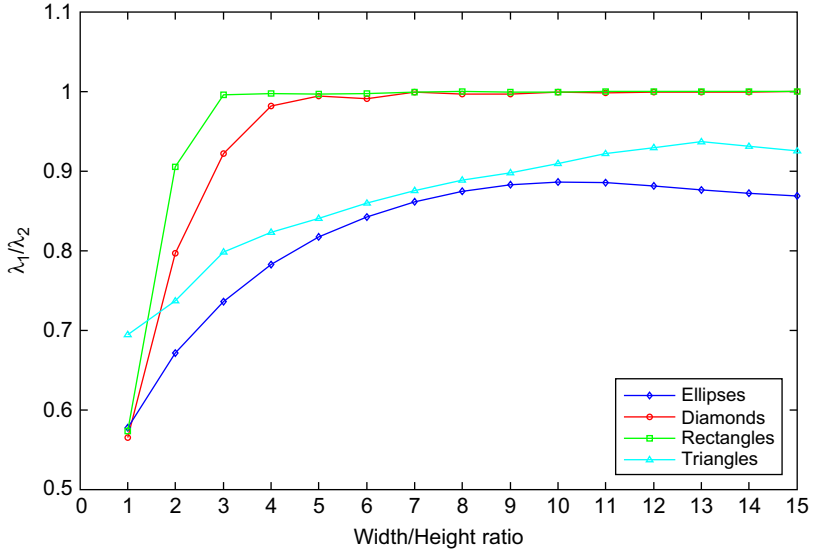

(a)

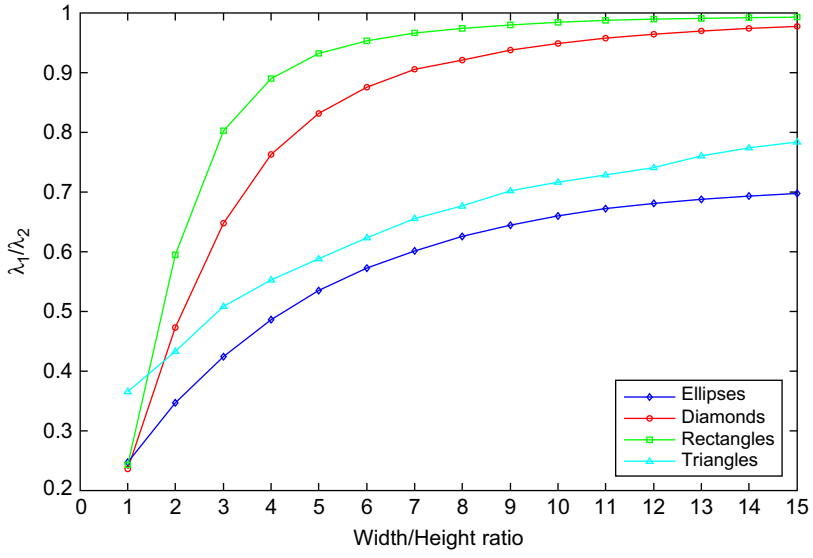

(b)

FIGURE 3 λ_1/λ_2 for basic shapes of varying aspect ratios: (a) buckling, (b) clamped plate.

is enough to differentiate between the four simple shapes considered. For the buckling problem, the ratio Λ_2/Λ_1 differentiates triangles and diamonds but has the same asymptotic behavior for rectangles and ellipses as the aspect ratio becomes large.

Figures 4 and 5 show the graphs of λ_3/λ_1 versus λ_2/λ_1 for each of the simple shapes, and for each of the operators considered. Assuming no prior knowledge about the aspect ratio, Figure 4a, corresponding to the Dirichlet case, shows that while knowledge of the ratio $\frac{\lambda_2(\Omega)}{\lambda_1(\Omega)}$ is not enough to know the shape of the domain Ω, the pair $(\lambda_2/\lambda_1, \lambda_3/\lambda_1)$ can easily differentiate between rectangles, ellipses, and triangles. This phenomenon is similar in the case of the clamped and buckling problems shown in Figure 5. While Dirichlet, clamped, and buckling eigenvalues tend to confuse "bulky" diamonds and rectangles, Neumann eigenvalues tend to confuse thin long triangles and ellipses. These aspects are shown in Figures 4–6 as well as in Figures 6 and 7 where graphs for λ_3/λ_2 vs. λ_2/λ_1 are treated.

The graphs that optimize λ_3/λ_1 versus λ_2/λ_1, and similar considerations, have been discussed abundantly in earlier work (see Ashbaugh and Benguria, 1994b,c; Levitin and Yagudin, 2003). The case of rectangles is explicitly discussed in these references. Suffice to say that the maximum value for the case of rectangles in Figure 4a corresponds to the ratios $(20/11, 35/11)$ which matches on the graph obtained using the 5-point finite difference scheme described below. The maximum value of λ_2/λ_1 is, of course, 2.539, which checks as well with what is known theoretically. In this case, $\lambda_2 = \lambda_3$. These numbers check in Figure 6a as well, where the maximum λ_2/λ_1 for the disk corresponds to the point $(2.539, 1)$. The extremal among all rectangles in Figures 5a and 6a is also the extremal among all diamonds and corresponds to the most symmetric of these membranes—namely, the square—for which $\lambda_2/\lambda_1 = 2.5$ for which also $\lambda_2 = \lambda_3$. Graphs for the various classes of basic shapes exhibit similar behavior for the Dirichlet, clamped, and buckling cases, raising curious questions thus far not treated in the theoretical literature for the clamped and buckling problems. Note also that when λ_2/λ_1 increases, corresponding to more symmetric membranes, the feature vectors for the Dirichlet, clamped, and buckling problems do not distinguish much between rectangles and diamonds. This is not the case of the Neumann problem where clearly, in Figures 4b and 5b rectangles and diamonds, and in fact all the basic shapes can be separated, except elongated triangles and ellipses with large aspect ratios. There is a trade-off between Dirichlet, clamped, and buckling features and those of Neumann case that warrants closer future considerations. The vertical line at 4 for these two graphs confirms the Ashbaugh and Benguria conjecture. This is also displayed in Figure 9 where the asymptotic line becomes horizontal and still corresponds to elongated rectangles (see Antunes & Henrot, 2011). In Figure 8,

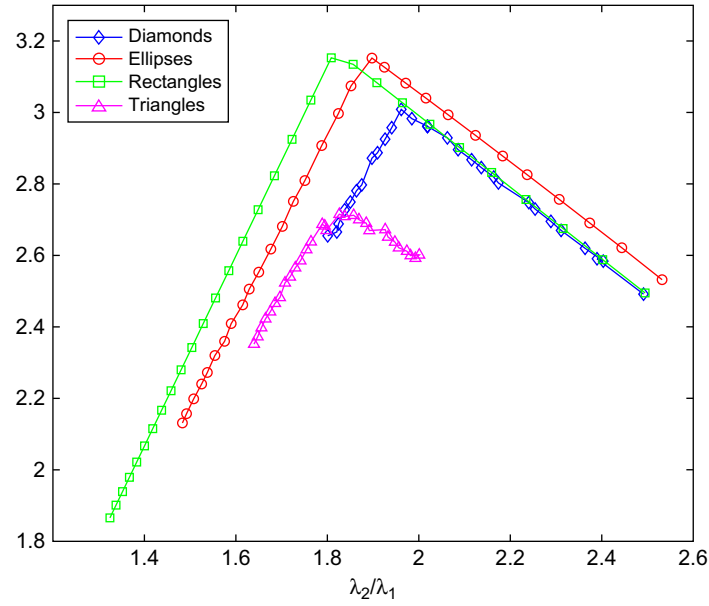

(a) Dirichlet

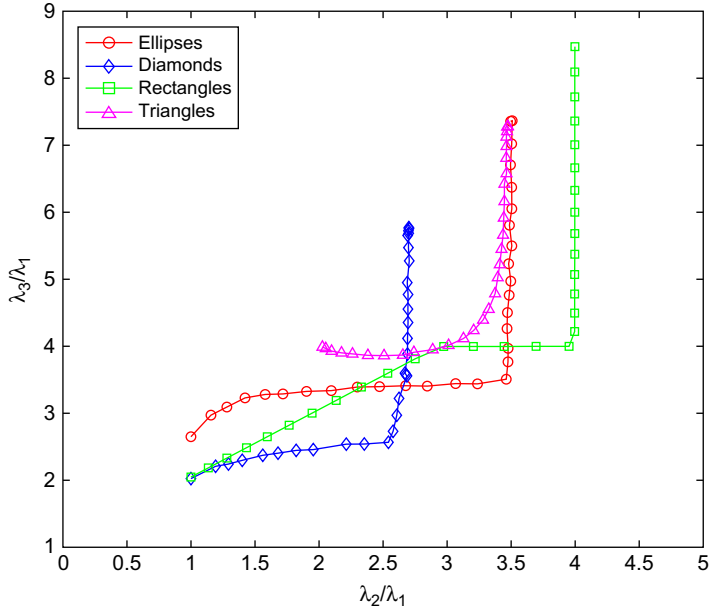

(b) Neumann

FIGURE 4 Ratios λ_3/λ_1 versus λ_2/λ_1 for each operator.

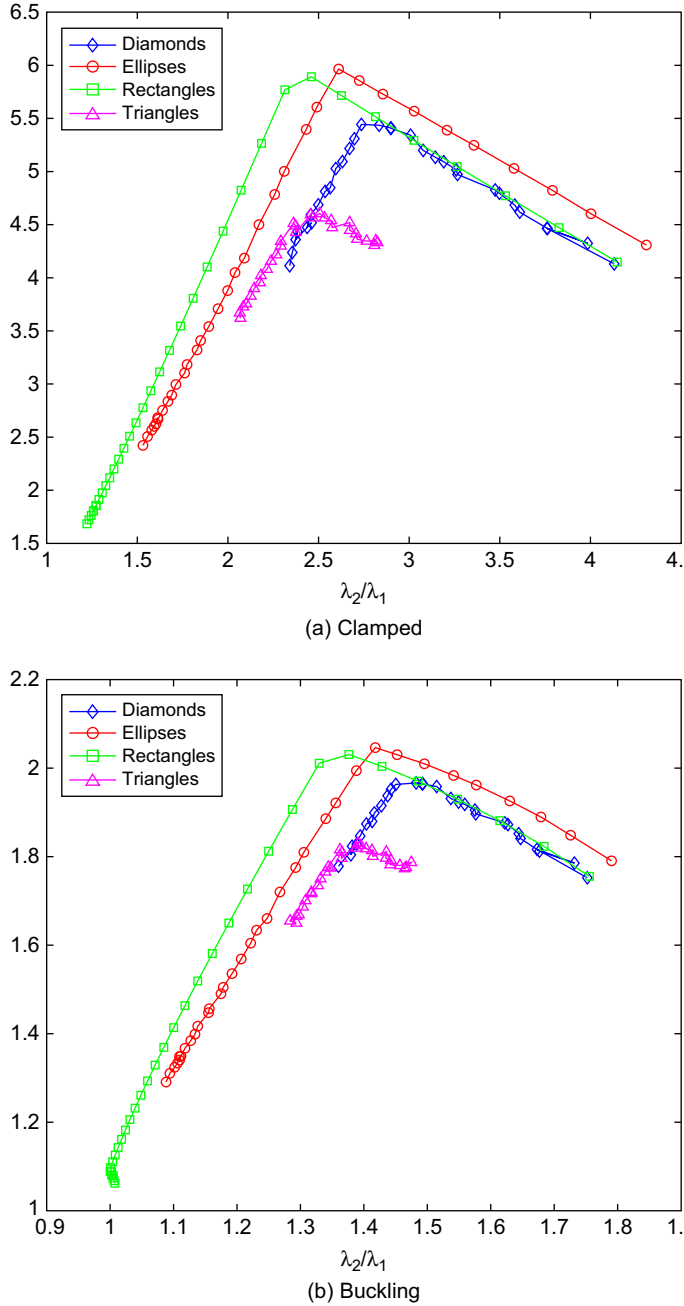

FIGURE 5 Ratios λ_3/λ_1 versus λ_2/λ_1 for each operator.

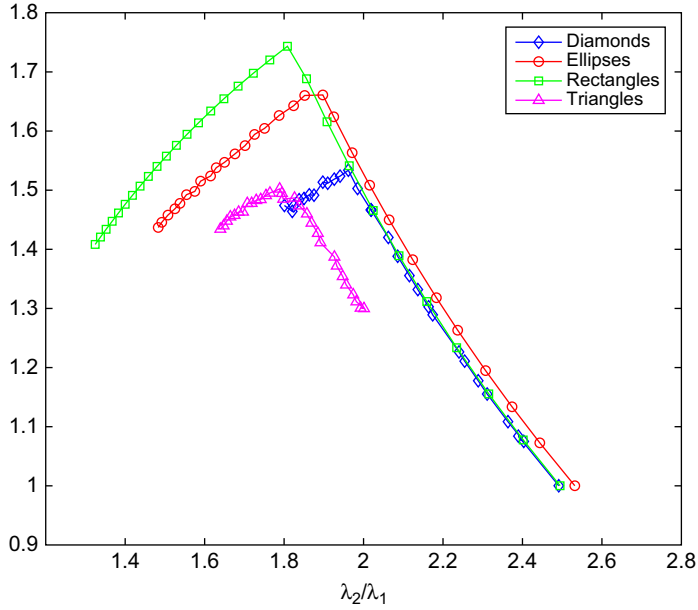

(a) Dirichlet

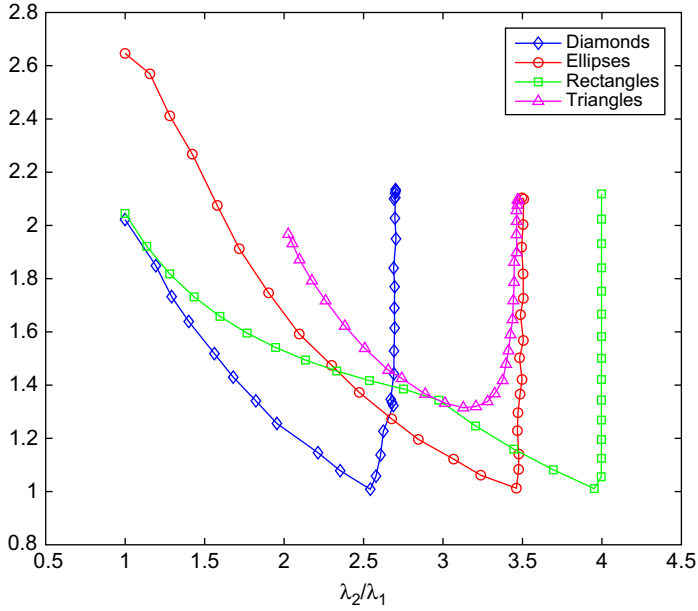

(b) Neumann

FIGURE 6 Ratios λ_3/λ_2 versus λ_2/λ_1 for each operator.

the maximum λ_2/λ_1, among all simple shapes considered, corresponds to a disk. The case of the Neumann problem considered in Figure 9 suggests disks minimize the ratio μ_3/μ_2, at least among the simple convex shapes considered.

The numbers for the clamped and buckling problems check as well at the level of the rudimentary finite difference method we are using in this work. The optimal value of Γ_2/Γ_1 is obtained for a square plate and has a value around 4.1597 (see Fichera, 1967). This is as observed in Figures 5a, where we note that $\Gamma_2 = \Gamma_3$ in this case, and Figure 7a. For the circular plate, the graphs show the optimal value of about 4.3311 for Γ_2/Γ_1, for which we also observe that $\Gamma_2 = \Gamma_3$ (see Figure 7a).

In the case of the buckling problem, (Aimi & Diligenti, 1992, 1994) give a value of about 1.7599 for a square plate. This is displayed in Figures 5b and Figure 7b. Also for this case, $\Lambda_2 = \Lambda_3$. Clearly, for these simple shapes the optimal given by the graphs for Λ_2/Λ_1 is about 1.8, which is in tune with the inequalities (4.23) and (4.24). At the optimal Λ_2/Λ_1, $\Lambda_2 = \Lambda_3$ for the case of ellipses, rectangles, and diamonds (see Figure 7b).

The extremal values for Γ_2/Γ_1, Λ_2/Λ_1, and μ_3/μ_2 also check in Figures 8 and 9, where for the clamped and buckling problems diamonds and triangles are confused part of the time, and in the case of Neumann, elongated triangles and ellipses with large aspect ratios are also confused. It is clear that there is a strong, at least heuristically, correlation between the Dirichlet, clamped, and buckling problems that warrants further work. For the simple shapes considered, rectangles play a special role in Figures 8 and 9, producing the smallest λ_2/λ_1, Λ_2/Λ_1, Γ_2/Γ_1, and largest μ_3/μ_2. The ratio of the fundamental tones of the Dirichlet, clamped, and buckling problems is maximal in all cases of basic shapes, when the membrane is circular. For the Neumann problem, the ratio of the first two nonzero fundamental tones is minimal for a symmetric shape, which is the case of squares and disks displayed, respectively, at the points $(2.5, 1)$ and $(2.539, 1)$ in Figure 9.

6. COMPUTATION OF THE EIGENVALUES

6.1. The Discrete Laplacian

Richardson (1910), Collatz (1938), Courant (1943), and Pólya (1952) are credited with inventing the finite difference scheme (Bramble and Hubbard, 1968; Hubbard, 1961; Forsythe, 1954, 1955; Forsythe and Wasow, 2004; Kuttler & Sigillito, 1984; Kuttler, 1970a; Pólya, 1952b, 1954; Weinberger, 1956, 1958, 1974). The short note from Oden (1990) makes a connection with the finite element literature and gives a beautiful overview of the contributors to the finite difference/finite element formulation of the Laplacian eigenvalue value problem, tracing it back to Schellbach (1851)

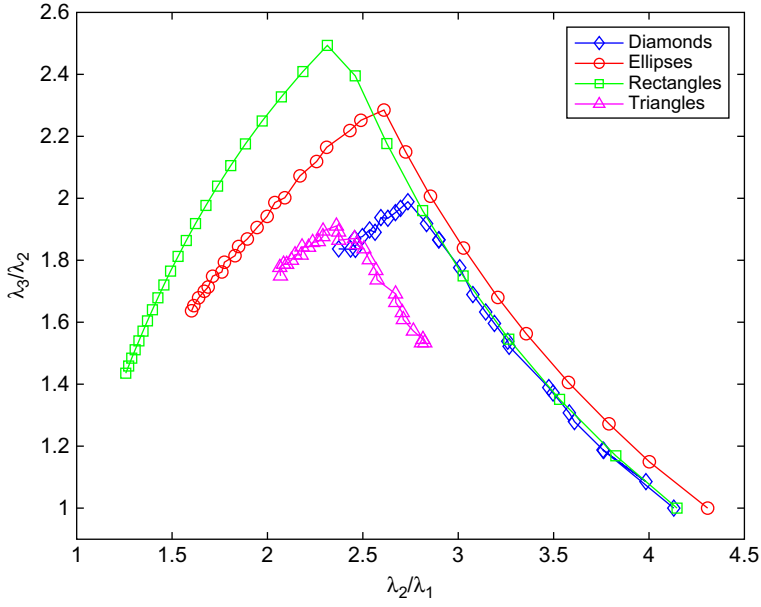

(a) Clamped

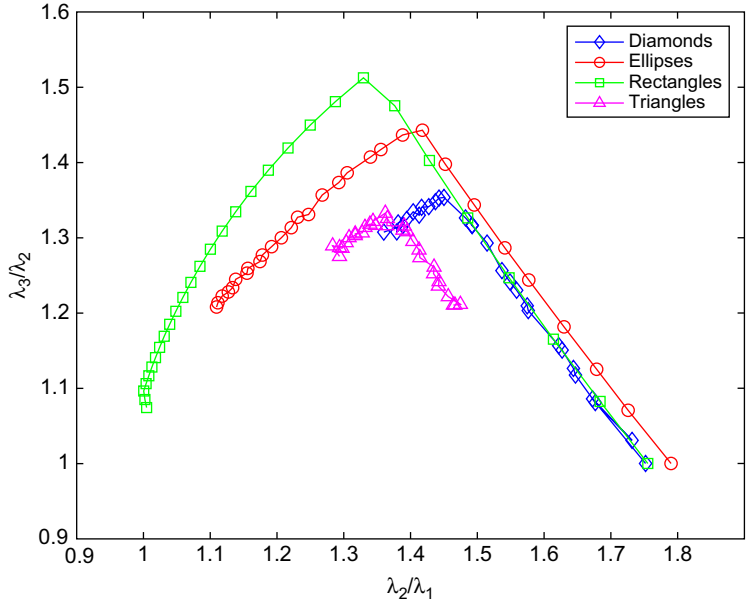

(b) Buckling

FIGURE 7 Ratios λ_3/λ_2 versus λ_2/λ_1 for each operator.

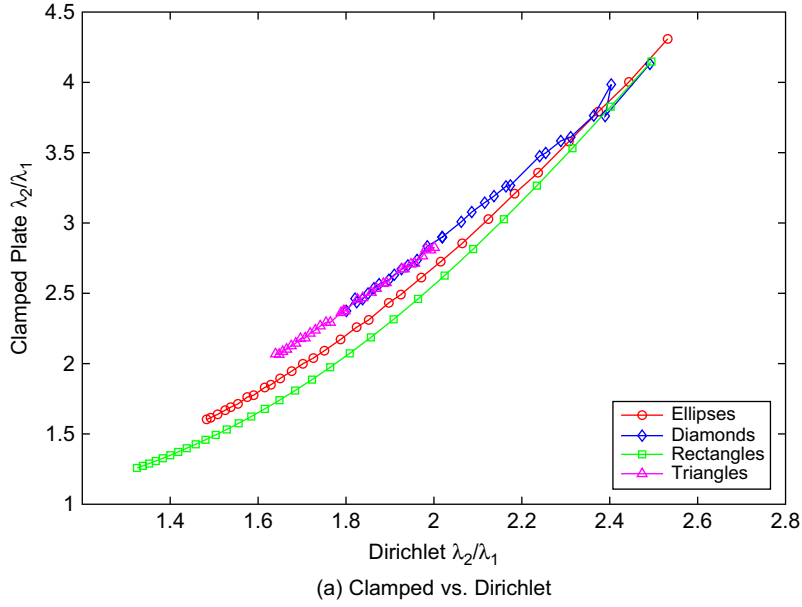

(a) Clamped vs. Dirichlet

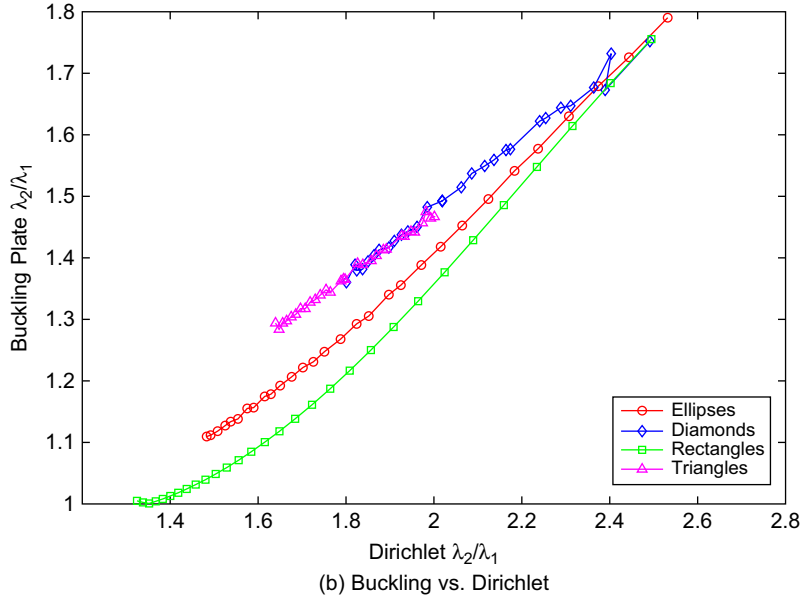

(b) Buckling vs. Dirichlet

FIGURE 8 Comparing λ_2/λ_1 for various operators.

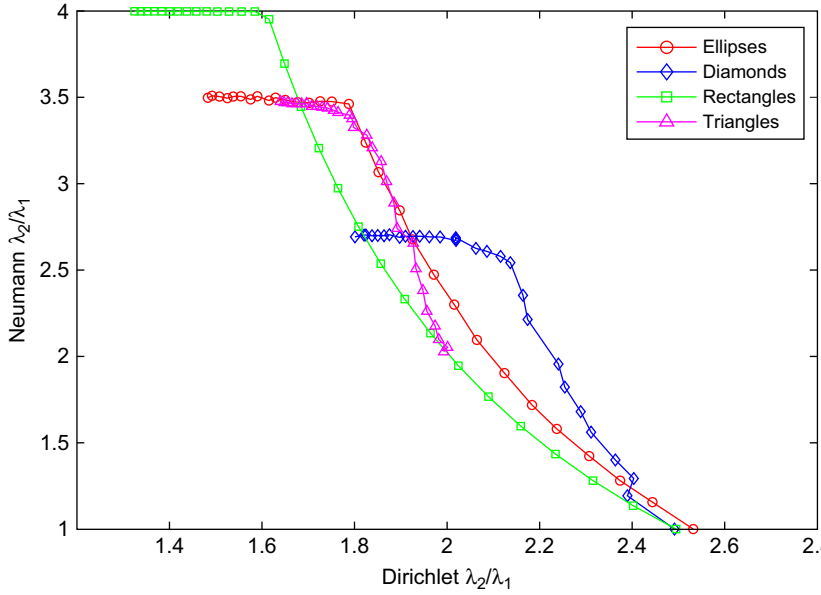

FIGURE 9 Neumann λ_2/λ_1 vs. Dirichlet λ_2/λ_1.

and even farther back to Bernoulli and Leibniz. Geometers and computer scientists trace the combinatorial discrete formulation of the Laplacian to Maxwell (1864) and Cremona (1874) Grinspun, Kälberer, Mathur, & Wardetzky (2007). One should also mention Moler's 1965 doctoral thesis under Forsythe, which treated the rate of convergence of the discretized eigenvalue problem to the original continuous one for the case of the Dirichlet problem when the size of the mesh goes to zero, Moler (1965), and the influential books by Forsythe and Wasow (2004) and Strikwerda (2004) which focus solely on finite difference schemes and provide good introductions to various fundamental questions of finite difference schemes such as stability, accuracy, and well-posedness.

6.2. Basic 5-Point Scheme and Dealing with the Boundary Conditions

There are many ways to discretize and compute the eigenvalues of the Laplacian. We use the finite difference method for our purposes. This is the oldest and most "natural" way of discretizing the Laplacian operator. This procedure is obtained by laying a mesh or grid of rectangles, squares, or triangles in the plane. The tessellation thus obtained generates nodes. We are interested in the nodes that fall inside the domain Ω. Mathematicians have devised different ways of dealing with the boundary $\partial\Omega$ and with

the boundary condition at hand. We first describe the discretization of the Laplacian and then briefly note some ways authors have dealt with the boundary conditions.

The value of the Laplacian of a function $u(x, y)$ at a given node is approximated by a linear combination of the values of the function at nearby nodes. For example, for a square mesh of width h, the 5-point finite difference approximation of order $O(h^2)$ is given by

$$\Delta_h u := \frac{u(x+h,y) + u(x-h,y) + u(x,y+h) + u(x,y-h) - 4u(x,y)}{h^2}.$$

A given shape can then be thought of as a pixelated image, with h being the width of a pixel. By Taylor expansion, it is clear that

$$\Delta u - \Delta_h u = O(h^2).$$

In practical terms, after discretization, with u_{ij} representing the value of u at the lattice point (ih, jh), one has

$$(\Delta_h u)_{i,j} = \frac{1}{h^2}(u_{i+1,j} + u_{i,j+1} + u_{i-1,j} + u_{i,j-1} - 4u_{ij}).$$

Symbolically, numerical analysts write it in the form

$$\Delta_h = \frac{1}{h^2}\begin{pmatrix} & 1 & \\ 1 & -4 & 1 \\ & 1 & \end{pmatrix}.$$

The eigenvalue problem is replaced by a matrix eigenvalue problem

$$\begin{aligned} -\Delta_h u &= \lambda^h u \quad \text{in} \quad \Omega_h \\ u &= 0 \quad \text{on} \quad \partial\Omega_h, \end{aligned} \tag{6.1}$$

with eigenmodes defined by $0 < \lambda_1^h < \lambda_2^h \leq \lambda_3^h \leq \cdots \leq \lambda_{N_h}^h$. Here N_h is commensurable with the number with pixels inside Ω_h (see Khabou et al., 2007a; Zuliani et al., 2004).

The finite difference stencil is a compact graphical way to represent the chosen finite difference scheme. The stencil for the 5-point finite difference scheme is shown in Figure 10.

Notice that these eigenvalues satisfy a discrete version of the Courant–Fischer minimax principle:

$$\lambda_k^h = \inf_{u_1,u_2,\ldots,u_k} \sup_{a_1,a_2,\ldots,a_k} \frac{h^2 \sum_{i=1}^2 \sum_{\Omega_h} (\partial_i (a_1u_1 + a_2u_2 + \cdots + a_ku_k))^2}{h^2 \sum_{\Omega_h} (a_1u_1 + a_2u_2 + \cdots a_ku_k)^2}. \tag{6.2}$$

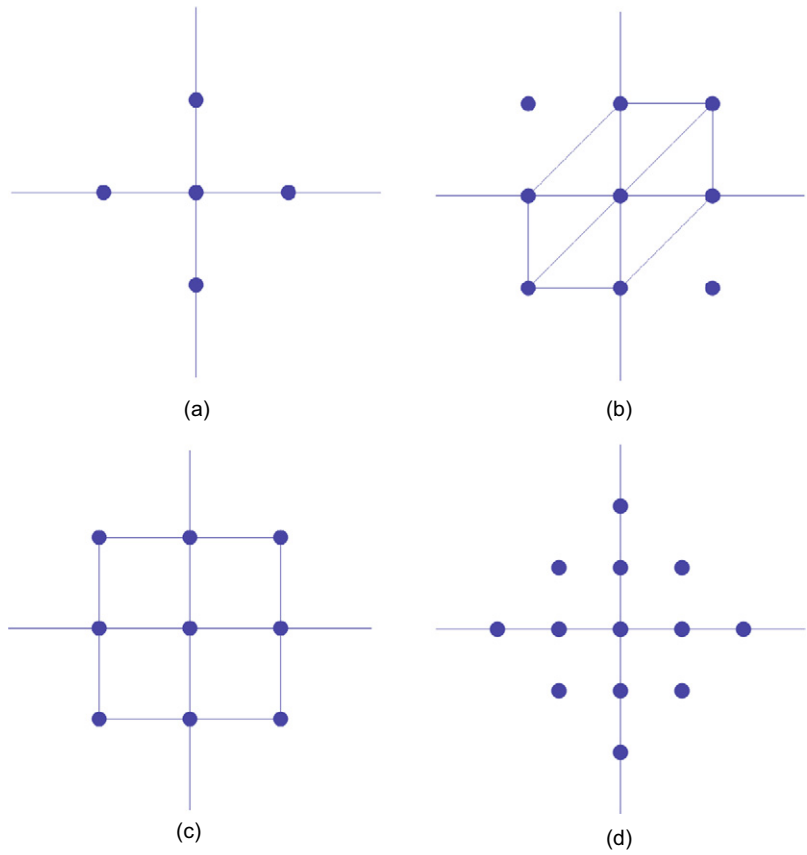

FIGURE 10 Stencils for various finite difference Laplacian schemes: (a) 5-point scheme; (b) 7-point-scheme; (c) 9 point scheme; (d) basic 13-point scheme for the bi-Laplacian.

Here ∂_i denotes the forward difference operator in the ith component, for $i = 1, 2$,

$$\partial_1 u(x,y) = u(x+h,y) - u(x,y) \quad \text{and} \quad \partial_2 u(x,y) = u(x,y+h) - u(x,y),$$

and $u_1, u_2, \ldots, u_k$ are linearly independent mesh functions vanishing everywhere except in Ω_h.

Forsythe proved, Forsythe (1954, 1955); Forsythe and Wasow (2004) that there exists $\gamma_1, \gamma_2, \ldots, \gamma_k, \ldots$, etc, such that

$$\lambda_k^h \leq \lambda_k - \gamma_k h^2 + o(h^2).$$

Moreover, the γ_k's cannot be computed but are positive when Ω is convex. Keller derived in 1965 a general result, Keller (1965), that provides a

bound for the difference between the computer and theoretical eigenvalues for the Dirichlet eigenvalue problem from knowledge of the estimates on the truncation error, under a technical condition between the boundaries $\partial\Omega_h$ and $\partial\Omega$. If

$$\tau_h(u(x,y)) := (\Delta - \Delta_h)u(x,y)$$

denotes the *local truncation error*, for a given function u, at a point $(x,y) \in \Omega_h$, then for each λ_k eigenvalue of the continuous problem, there exists λ^h eigenvalue of the difference problem, such that

$$|\lambda_k - \lambda^h| \leq \frac{\|\tau(u_k)\|_2}{\|u_k\|_2}.$$

Effects of boundary regularity for the 5-point discretization of the Laplacian were treated by (Bramble and Hubbard) in 1968 (see also Moler, 1965). When the equation of the boundary in local coordinates is twice differentiable and the second derivatives satisfy a Hölder condition,

$$|\lambda_k - \lambda_k^h| \leq K h^2.$$

A similar result holds for the maximum difference between the eigenfunction and its discretized equivalent. More complicated situations are treated in Bramble and Hubbard (1968) and Moler (1965). Weinberger (1958) proved that

$$\lambda_k^h \leq \frac{\lambda_k}{1 - \frac{h^2}{k^2}\lambda_k},$$

from which it follows that

$$\frac{\lambda_k^h}{1 + \frac{h^2}{\pi^2}\lambda_k^h} \leq \lambda_k.$$

An upper bound result that complements this is provided by Kuttler, who showed in 1970 that

$$\lambda_k \leq \frac{\lambda_k^h + \frac{1}{12}h^2(\lambda_k^h)^2 + \frac{1}{168000}h^8(\lambda_k^h)^5 + \frac{1}{1334000}h^{10}(\lambda_k^h)^6}{1 - \frac{1}{40}h^4(\lambda_k^h)^2 - \frac{1}{560}h^6(\lambda_k^h)^3}, \tag{6.3}$$

an inequality that improves an earlier result of Weinberger (1958)

$$\lambda_k \leq \frac{\lambda_k^h}{1 - \frac{1}{4}h^2\lambda_k^h}, \tag{6.4}$$

viz., that the bound in (6.3) is asymptotically equal to

$$\lambda_k^h + \frac{1}{12}h^2(\lambda_k^h)^2 + \frac{1}{40}h^4(\lambda_k^h)^3 + \cdots,$$

while that in (6.4) has the expansion

$$\lambda_k^h + \frac{1}{4}h^2(\lambda_k^h)^2 + \frac{1}{16}h^4(\lambda_k^h)^3 + \cdots.$$

Burden and Hedstrom (1972) proved a remarkable discrete version of the Weyl asymptotic formula for the case of the 5-point scheme.

Hubbard (1961) performed most of the analysis for the Neumann finite difference scheme using the 5-point formulation described above:

$$\Delta_h\, v = \mu^h\, v,$$

and the normal boundary condition is given (for boundary pixels) by

$$v_{i,j} = \text{ average of adjacent "interior" points.}$$

For example, for a boundary point on the left of a planar domain, we write

$$v_{i,j+1} + v_{i+1,j} + v_{i,j-1} = 3v_{i,j}.$$

Using a slightly weaker formula of the minimax principle, Hubbard (1961) derived formulas similar to those of Weinberger and Kuttler carefully relating the eigenvalues to curvature integrals.

The new edition of Strikwerda's indispensable book on finite difference schemes Strikwerda (2004) offers a brief new section (Section 13.2) that shows how to explicitly calculate the Dirichlet eigenvalues for a 5-point discretization when Ω is the rectangle using a discrete version of the techniques of separation of variables and recursion techniques (see also Burden and Hedstrom, 1972).

6.3. Higher-Order Discretizations of the Laplacian

To circumvent the problem of not being clear about the behavior of the approximate eigenvalues compared with the exact ones, Pólya (1952b, 1954) (see also Forsythe and Wasow, 2004) proposed two modifications. In both cases, he suggested generalized eigenvalue problems of the form

$$\mathcal{L}_{ij}\, u = \lambda\, \mathcal{R}_{ij}\, u,$$

where $\mathcal{L}_{ij}$ and $\mathcal{R}_{ij}$ take various forms depending on the modification. To further the mechanical analogy, $\mathcal{L}_{ij}$ and $\mathcal{R}_{ij}$ are usually thought of as elements of the stiffness and mass matrices in a system of springs in which the mesh points are thought of as a chain of masses carrying different weights linked by springs with different constants. In the 5-point scheme case,

$$\mathcal{L}_{ij}\, u = \frac{1}{h^2}\left(u_{i+1,j} + u_{i,j+1} + u_{i-1,j} + u_{i,j-1} - 4\, u_{ij}\right),$$

and $\mathcal{R}_{ij} =$ identity.

In the first modification, Pólya (1952b) proposed to change $\mathcal{R}_{ij}$ to

$$\mathcal{R}_{ij}\, u = -\frac{1}{12}\left(6u_{ij} + u_{i+1,j} + u_{i,j+1} + u_{i-1,j} + u_{i-1,j-1} + u_{i,j-1}\right).$$

This takes the simplified 7-point scheme represented by the stencil in Figure 10b, where the stiffness and mass are given by

$$-\frac{1}{h^2}\begin{pmatrix} & 1 & \\ 1 & -4 & 1 \\ & 1 & \end{pmatrix} u = \frac{\bar{\lambda}^h}{12}\begin{pmatrix} 1 & 6 & 1 \\ 1 & 1 & \end{pmatrix} u \text{ in } \Omega_h$$

$$u = 0 \text{ on } \partial\Omega_h.$$

This scheme satisfies the property

$$\lambda_k \le \bar{\lambda}_k^h \le \frac{\lambda_k}{1 - \frac{1}{4}h^2\lambda_k}$$

proved by Weinberger (1956, 1958), which provides two-sided bounds for the eigenvalues of the membrane problem, namely,

$$\frac{\bar{\lambda}_k^h}{1 + \frac{1}{4}h^2\bar{\lambda}_k^h} \le \lambda_k \le \bar{\lambda}_k^h.$$

It is then clear that in this case $\bar{\lambda}_k^h - \lambda_k = O(h^2)$.

In the second modification, Pólya (1952b) proposed to replace both $\mathcal{L}_{ij}$ and $\mathcal{R}_{ij}$ with

$$\mathcal{L}_{ij}\, u = \frac{1}{3h^2}\left(u_{i+1,j} + u_{i+1,j+1} + u_{i,j+1} + \cdots + u_{i+1,j-1} - 8u_{ij}\right)$$

and

$$\mathcal{R}_{ij}\, u = -\frac{1}{36}\,(16u_{ij} + 4u_{i+1,j} + 4u_{i,j+1} + 4u_{i-1,j} + 4u_{i,j-1} + u_{i+1,j+1} + u_{i+1,j-1} + u_{i-1,j+1} + u_{i-1,j-1}).$$

This amounts to a recursive scheme with stiffness and mass matrices elements given by

$$-\frac{1}{3h^2}\begin{pmatrix}1 & 1 & 1\\ 1 & -8 & 1\\ 1 & 1 & 1\end{pmatrix} u = \frac{\bar{\lambda}^h}{36}\begin{pmatrix}1 & 4 & 1\\ 4 & 16 & 4\\ 1 & 4 & 1\end{pmatrix} u \text{ in } \Omega_h$$
$$u = 0 \text{ on } \partial\Omega_h$$

with a full 9-point scheme represented by Figure 10c. This 9-point scheme satisfies the property $\lambda_k \le \bar{\lambda}_k^h$ as well. Moreover, Lyashenko, Meredov, and Embergenov (1984) proved that the 5-point and 9-point schemes can be obtained to obtain a better approximation of the eigenvalues for the continuous case,

$$\frac{\lambda_k^h + \bar{\lambda}_k^h}{2} = \lambda_k + O(h^4),$$

when Ω is strictly convex with C^1 boundary, where λ_k^h denotes the eigenvalue emanating from the 5-point scheme.

6.4. Clamped Plate and Buckling of Clamped Plate Discretizations

A 13-point scheme naturally arises in discretizing the bi-Laplacian Δ^2 by successively applying the 5-point Laplacian described earlier: $\Delta_h^2 u = \Delta_h\,(\Delta_h u)$. In this case, one gets

$$\begin{aligned} h^4\,\Delta_h^2 u = {} & u(x,y-2h) + 2u(x-h,y-h) - 8u(x,y-h) + 2u(x+h,y-h)\\ & + u(x-2h,y) - 8u(x-h,y) + 20u(x,y)\\ & - 8u(x+h,y) + u(x+2h,y) + 2u(x-h,y+h)\\ & - 8u(x,y+h) + 2u(x+h,y+h) + u(x,y+2h). \end{aligned} \tag{6.5}$$

With u_{ij} denoting again the value of u at a lattice point (ih, jh), the bi-Laplacian takes the form

$$\begin{aligned} h^4 \left(\Delta_h^2 u\right)_{ij} = {} & u_{i,j-2} \\ & + 2u_{i-1,j-1} - 8u_{i,j-1} + 2u_{i+1,j-1} \\ & + u_{i-2,j} - 8u_{i-1,j} + 20u_{i,j} \\ & - 8u_{i+1,j} + u_{i+2,j} + 2u_{i-1,j+1} \\ & - 8u_{i,j+1} + 2u_{i+1,j+1} + u_{i,j+2}. \end{aligned} \tag{6.6}$$

The stencil for this discretization of the bi-Laplacian is represented in Figure 10d and the stiffness matrix is then given by

$$\Delta_h^2 = \frac{1}{h^4} \begin{pmatrix} & & 1 & & \\ & 2 & -8 & 2 & \\ 1 & -8 & 20 & -8 & 1 \\ & 2 & -8 & 2 & \\ & & 1 & & \end{pmatrix}.$$

In the discrete setting, the clamped plate problem takes the form

$$\Delta_h^2 u = \Gamma^h u \text{ in } \Omega_h, \tag{6.7}$$

where the boundary pixels are subject to

$$u_{i,j} = 0$$

and

$$u_{i,j} = \text{ average of adjacent "interior" points.}$$

The case of the buckling plate takes the form

$$\Delta_h^2 u = \Lambda^h \Delta_h u \text{ in } \Omega_h \tag{6.8}$$

with similar boundary conditions and Δ_h denoting the 5-point discretization of the Laplacian. Each discrete problem has a finite positive sequence of eigenvalues, commensurable in number with the number of pixels inside Ω_h. They are usually denoted by

$$0 < \Gamma_1^h \le \Gamma_2^h \le \cdots \le \Gamma_k^h \le \cdots,$$

and

$$0 < \Lambda_1^h \leq \Lambda_2^h \leq \cdots \leq \Lambda_k^h \leq \cdots .$$

These eigenvalues are characterized by the discrete version of the corresponding the Courant–Fischer minimax principle for these problems, namely

$$\Gamma_k^h = \inf_{u_1,u_2,\ldots,u_k} \sup_{a_1,a_2,\ldots,a_k} \frac{h^2 \sum_{\Omega_h} (\Delta_h (a_1 u_1 + a_2 u_2 + \cdots + a_k u_k))^2}{h^2 \sum_{\Omega_h} (a_1 u_1 + a_2 u_2 + \cdots a_k u_k)^2}, \tag{6.9}$$

and

$$\Lambda_k^h = \inf_{u_1,u_2,\ldots,u_k} \sup_{a_1,a_2,\ldots,a_k} \frac{h^2 \sum_{\Omega_h} (\Delta_h (a_1 u_1 + a_2 u_2 + \cdots + a_k u_k))^2}{h^2 \sum_{i=1}^2 \sum_{\Omega_h} (\partial_i (a_1 u_1 + a_2 u_2 + \cdots a_k u_k))^2}. \tag{6.10}$$

Here ∂_i denotes the forward difference operator described earlier and $u_1, u_2, \ldots, u_k$ are linearly independent mesh functions vanishing everywhere except in Ω_h. Weinberger (1958) proved the first inequality relating the eigenvalues of Eq. (4.1) to those of Eq. (6.7):

$$\Gamma_k^h \leq \frac{\Gamma_k}{1 - \frac{h^2}{\pi^2} \Gamma_k^{1/2}},$$

which leads to the lower bound

$$\Gamma_k \geq \Gamma_k^h + \frac{(\Gamma_k^h)^{3/2} h^2}{\pi^2} + \frac{(\Gamma_k^h)^2 h^4}{2\pi^4} + \frac{(\Gamma_k^h)^{5/2} h^6}{8\pi^6} + \cdots .$$

Using the method of Weinberger (1958), Kuttler (1970b) found further upper and lower bounds for the eigenvalues of the continuous problems in terms of those of Eqs. (6.7) and (6.8):

$$\frac{\Gamma^h}{1 + \frac{h^2}{\pi^2} \Gamma_k^h} \leq \Gamma_k \leq \frac{\Gamma_k^h + \frac{1}{2} h^2 (\Gamma_k^h)^{3/2}}{1 - \frac{1}{40} h^4 \Gamma_k^h - \frac{1}{560} h^6 (\Gamma_k^h)^{3/2}}, \tag{6.11}$$

and

$$\frac{\Lambda_k^h}{1 + 8\frac{h^2}{\pi^2} \Lambda_k^h} \leq \Lambda_k \leq \frac{\Lambda_k^h + \frac{1}{2} h^2 (\Lambda_k^h)^2}{1 - \frac{1}{120} h^4 (\Lambda_k^h)^2 - \frac{1}{2240} h^6 (\Lambda_k^h)^3}. \tag{6.12}$$

These inequalities clearly show that as $h \to 0$, the eigenvalues of the discrete problems converge to those of the continuous case. For the discretizations considered in this paper, we used the 5-point scheme for the Dirichlet and Neumann problems and the 13-point scheme for the case of clamped and buckling problems.

6.5. Other Methods of Computing the Eigenvalues

Rather than providing a comprehensive review of methods of computation of the eigenvalues of the membrane problem and the other associated problems described previously, we mention the techniques that were most prominent recently and others that provide future hope. The "bread and butter" of the bulk of the work of Reuter *et al.* has been the *finite elements method* (Niethammer et al., 2007; Peinecke et al., 2007; Reuter, 2010; Reuter et al., 2005a,b, 2009b). This is the method preferred in the work of Levitin and Yagudin (2003). Of particular interest to the computational community in recent years is the *method of particular solutions (MPS)* of Fox, Henrici, & Moler (1967), one of the most influential works in numerical analysis. MPS has received a recent "revival" thanks to work of Betcke and Trefethen (2005); Trefethen and Betcke (2006) (see also Guidotti and Lambers, 2008). Conformal techniques used by Driscoll (1997) proved very efficient in providing the first high-accuracy verification of the isospectrality of Bilby and Hawk. Improving a truncation estimate of Moler and Payne (1968) recently allowed (Barnett, 2009) to pursue high-lying eigenvalues with great numerical accuracy. Some of these techniques have roots in *collocation*, a technique devised by Collatz in the 1930s. We also note the *method of fundamental solution* as another popular method used to verify and produce conjectures as in the work of Antunes and Freitas (2006) and Antunes and Henrot (2011). By entirely avoiding the necessity of dealing with the boundary conditions, Saito (2008) discovered a new way of extracting geometric features from an integral operator based on Green's function of the entire space that is required to commute with the Laplacian, leading to a nonlocal boundary condition. Last, but not least, one should mention that in the case of the bi-Laplacian, Fichera (1967) and Weinstein (1937, 1966) have devised the most technically difficult methods to implement, which have the advantage of yielding the most accurate values known in the literature thus far. These methods provide two-sided bounds for the eigenvalues. Although interest in these methods has somewhat waned, the school is still active (see Aimi & Diligenti, 1992, 1994). Fichera's techniques also are in need of a "revival" since they provide highly accurate two-sided bounds for the difficult clamped and buckling problems and show numerically the slow convergence of the Weyl asymptotic formula Fichera (1967) (see also Weinberger, 1999).

7. FEATURES BASED ON THE EIGENVALUES OF THE VARIOUS PROBLEMS CONSIDERED

Given a planar domain Ω and a set of the first positive eigenvalues

$$0 < \lambda_1 \leq \lambda_2 \leq \cdots \leq \lambda_n\,,$$

for either of the previously described operators, we defined in Khabou et al. (2007a) the three feature vectors given by

$$F_1(\Omega) = \left(\frac{\lambda_1}{\lambda_2}, \frac{\lambda_1}{\lambda_3}, \frac{\lambda_1}{\lambda_4}, \ldots, \frac{\lambda_1}{\lambda_n}\right),$$

$$F_2(\Omega) = \left(\frac{\lambda_1}{\lambda_2}, \frac{\lambda_2}{\lambda_3}, \frac{\lambda_3}{\lambda_4}, \ldots, \frac{\lambda_{n-1}}{\lambda_n}\right),$$

and

$$F_3(\Omega) = \left(\frac{\lambda_1}{\lambda_2} - \frac{d_1}{d_2}, \frac{\lambda_1}{\lambda_3} - \frac{d_1}{d_3}, \frac{\lambda_1}{\lambda_4} - \frac{d_1}{d_4}, \ldots, \frac{\lambda_1}{\lambda_n} - \frac{d_1}{d_n}\right).$$

Here $d_1 \leq d_2, \ldots \leq d_n$ are the first n eigenvalues of a disk. Obviously the three feature vectors are translation, rotation, and scaling invariant. Moreover, the entries of each feature vector are all bounded, which makes them very suitable for all sorts of algorithmic manipulations. The feature vector F_3 somehow measures the *distance* of a domain Ω from a disk. In this chapter, we also introduce a fourth feature vector, namely

$$F_4(\Omega) = \left(\frac{\lambda_2}{\lambda_1}, \frac{\lambda_3}{2\lambda_1}, \frac{\lambda_4}{3\lambda_1}, \ldots, \frac{\lambda_{n+1}}{n\lambda_1}\right).$$

The entries of F_4 are the inverses of those in F_1 except for the division with n, which is meant to scale down the Weyl growth and prevent the entries of the vector from becoming too large.

The multitude of universal properties discussed in previous sections guarantee that the entries of the feature vectors are positive and bounded, and thus suitable for algorithmic manipulations. In particular, bounded input is quite convenient for artificial neural networks, which we discuss next.

8. ARTIFICIAL NEURAL NETWORKS

By most accounts, the artificial neural network (ANN) idea was born in 1943, when McCulloch and Pitts published their well-known paper that

showed it was mathematically possible to create an interconnected network capable of solving any computable task. ANNs were inspired by the way the human brain learns and processes information. In fact, the structure of an ANN mimics that of a human brain: It is composed of a large number of highly interconnected simple processing elements (neurons) working in parallel to learn/solve a specific problem. The human brain contains somewhere between 10 billion and 100 billion neurons that are massively interconnected. A particular neuron receives weighted stimuli from other neurons and simply "fires" (or not) depending on the total strength of the stimulus it receives. In a way, a neuron acts like a primitive processor with many inputs and one output, where its output y can be expressed as:

$$y = f\left(\sum_{i=0}^{\ell} x_i w_i\right),$$

where, $x_0 = 1$, w_0 is called the *neuron bias*, $x_1, \ldots, x_\ell$ are the stimuli from other neurons, and $w_1, \ldots, w_\ell$ are the weights of those stimuli (Figure 11). The function f, called the *activation function*, is typically a thresholding function:

$$f(x) = \begin{cases} 1 & \text{if } x > 0 \\ 0 & \text{if } x \leq 0. \end{cases}$$

Some ANN neurons use this type of activation function, but others use a continuous version of it, mainly

$$f(x) = \frac{1}{1 + e^{-a \sum_{i=0}^{\ell} x_i w_i}},$$

where $a > 0$.

The neurons in the human brain are interconnected in highly complicated and dynamic patterns with new connections established and

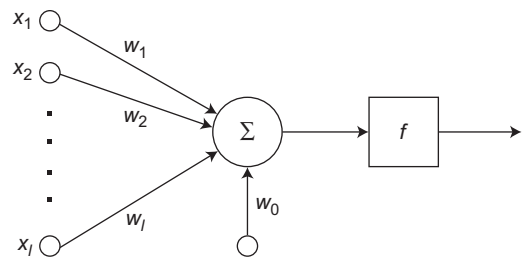

FIGURE 11 Neuron structure.

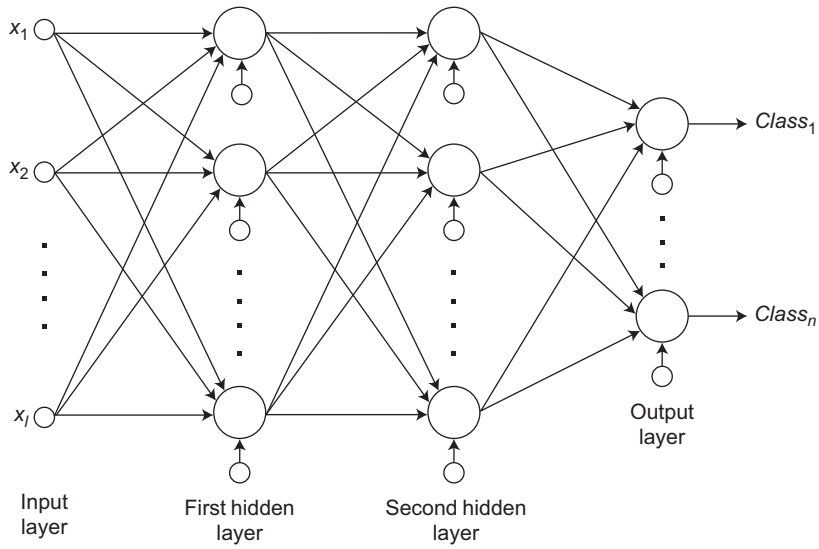

FIGURE 12 Feed-forward ANN composed of one input layer, two hidden layers, and one output layer.

old ones pruned as the brain develops and adapts. Similarly, several ANN structures exist with the "feed-forward" structure one of the most commonly used (Figure 12) (Haykin, 1994). A feed-forward structure is composed of a sea of neurons grouped into "layers." The first layer is the input layer where an input pattern is fed to the network. As input patterns are "fed-forward" to the middle layers (called *hidden layers*), information in the input patterns is mapped to other hyperspaces (possibly of higher dimensionality than the input space) where the patterns are "reorganized" before being fed to the final layer (called the *output layer*) where decision/approximation is made.

Like a human brain, an ANN can be trained to learn by example. Many ANN training strategies exist; however, the supervised backpropagation training algorithm is one of the most commonly used (Werbos, 1974; Rumelhart, Hinton, & Williams, 1986; Werbos, 1998). The backpropagation algorithm is a gradient descent method (Strikwerda, 2004) that iteratively updates the neurons' connection weights to optimize a cost function, typically chosen to be the least squares error between desired responses and actual responses of the network for a set of training patterns. More precisely, the training process tries to find the weights to minimize the cost function

$$J = \sum_{i=1}^{N} E(i),$$

where N is the total number of training samples and

$$E(i) = \frac{1}{2} \sum_{m=1}^{M} e_m^2(i)$$

is the difference between the desired and actual ANN output at the output layer for training sample i (M is the number neurons at that layer). The term $e_m^2(i)$ represents the difference between the desired and actual output at neuron m of the output layer. At every iteration of the training process, a training sample is presented to the ANN and its output is calculated using the current weight values. The difference between the desired and actual outputs is calculated and is used to proportionally update the weights starting at the output neurons and moving backwards toward the input neurons (Haykin, 1994). The training stops when the cost function reaches zero or stabilizes.

Neural network usage saw a huge boost in the 1980s and 1990s when computer power became adequate enough to simulate and train such massively connected structures. ANNs have been used in a variety of applications ranging from stock price prediction, robotics, quantum chemistry, to automatic target detection and recognition (Haykin, 1994; Poggio and Girosi, 1990). They are especially useful as pattern classifiers because of their fault tolerance, robustness, and universal function approximation ability (Sandberg, 1992). In theory, a multilayer feed-forward neural network with enough nodes and hidden layers can approximate any bounded function and its derivative to any arbitrary accuracy given a "large enough" training set (Hornik, Stinchrombe, & White, 1990). This property also means that a neural network can be used to separate patterns from different classes even if the classes are not linearly separable (i.e., no hyperplane exists that can separate patterns from the different classes). Another desired property of ANNs is their generalization capability. Generalization is a measure of how well a trained network performs on testing patterns not seen during the training process. For the aforementioned reasons, we decided to use feed-forward ANNs as classifiers in this work.

9. EXPERIMENTAL RESULTS

We conducted two sets of experiments to evaluate and compare the performance of the Dirichlet, Neumann, buckling plate, and clamped plate features. We used a variety of datasets in our experiments. Some were computer generated (CG), some were hand-drawn (HD), and some were extracted from a standard database of fish images. In the first set of experiments, we wanted to investigate the class separation capabilities of the

different features and their tolerance of boundary deformation. In the second set of experiments, we wanted to investigate the noise tolerance of the different features; particularly, we wanted to see how these features reacted to holes in the shapes and intruding and extruding noise at the boundary. The results of these experiments are described in the following sections.

9.1. Class Separation Capability and Tolerance of Boundary Deformation

A good feature set should react differently to images from different classes producing feature vectors that are very different from class to class. Another desirable property of a feature set is that only a "few" features are needed to discriminate between classes. Using fewer features allows the design of a simpler—and hence faster—classifier. Obviously, the number of features needed in a particular classification problem depends on the number of classes and their complexity. A good feature set should also be tolerant of some variations within a class. To test these properties in our proposed feature sets, we conducted two sets of experiments. The first set of experiments was conducted using simple hand-drawn and computer-generated images of disks, triangles, rectangles, ellipses, diamonds, and squares. The second set of experiments was conducted using a subset of natural shapes from a standard dataset of fish images.

9.2. Computer-Generated and Hand-Drawn Shapes

A total of 288 hand-drawn images of disks, triangles, rectangles, ellipses, diamonds, and squares of different sizes and orientations were scanned into the computer. Samples are shown in Figure 13. As can be seen from these samples, the boundaries of these shapes are noisy and irregular. The Dirichlet, Neumann, clamped-plate, and buckling plate eigenvalues of these hand-drawn images were computed and $n = 20$ F_1, F_2, F_3, and F_4 features from each group were generated. Next, we trained simple feed-forward neural networks with one hidden layer with $n = 4, 8, 12, 16$, and 20 features of 300 *computer-generated* images of disks, triangles, rectangles, ellipses, diamonds, and squares. The ellipses, rectangles, and diamonds had variable aspect ratios ranging from 2 to 2.5. The triangles were completely random. The trained neural networks were then tested using a *different* set of 300 computer generated pictures and the set of 288 *hand-drawn* shapes. We wanted to gauge the robustness of the features and their tolerance of noise and boundary deformation since the computer-generated shapes can be thought of as "noise-free" version of the hand-drawn shapes. Tables 1–4 summarize the results of these experiments. As clearly seen in the tables, we were able to attain very high

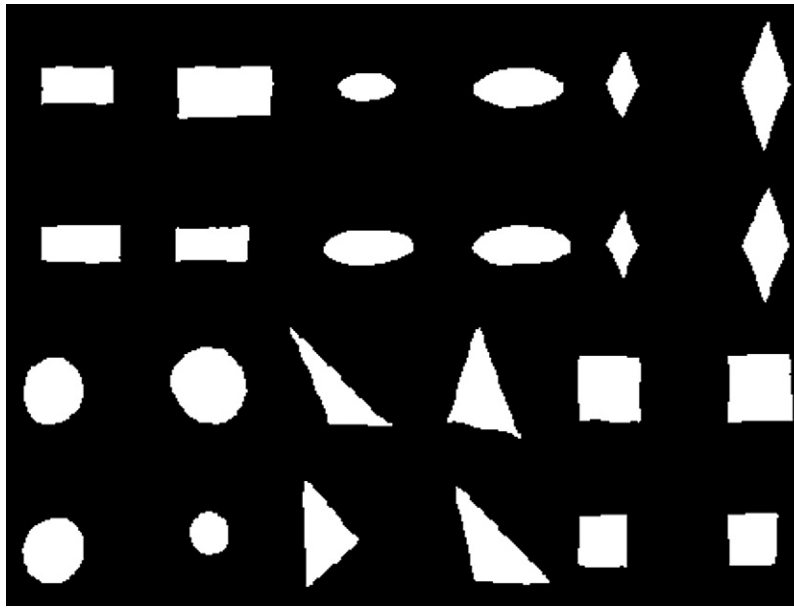

FIGURE 13 Sample hand-drawn shapes.

TABLE 1 Correct Classification Rates of Computer-Generated (CG) and Hand-Drawn (HD) Shapes Using Dirichlet Features

	F_1		F_2		F_3		F_4	
N	CG	HD	CG	HD	CG	HD	CG	HD
4	98.0	95.1	97.3	89.2	96.0	91.7	97.3	95.8
8	99.3	94.1	99.3	92.4	98.0	94.4	99.3	96.2
12	99.0	94.4	99.3	92.4	98.7	93.8	99.3	96.5
16	99.3	95.8	99.3	94.1	99.0	96.2	99.7	96.5
20	99.7	96.5	99.3	87.8	99.3	96.5	99.0	97.2
Average	**99.1**	**95.2**	**98.9**	**91.2**	**98.2**	**94.5**	**98.9**	**96.4**

classification rates (up to 100%) using all the feature sets. This testifies to the ability of all the feature sets (whether they are based on Dirichlet, Neumann, buckling, or clamped plate eigenvalues) to separate the six classes. Also, all feature sets proved to be tolerant of boundary variations and performed very well with both computer-generated and hand-drawn images. Moreover, all feature sets were able to achieve a high classification rate using only a small number of features (classification rates well above 90% using only 4 or 8 features). This is further evidence of these features' usefulness as shape classifiers.

TABLE 2 Correct Classification Rates of Computer-Generated (CG) and Hand-Drawn (HD) Shapes Using Neumann Features

	F_1		F_2		F_3		F_4	
N	CG	HD	CG	HD	CG	HD	CG	HD
4	99.0	93.1	99.0	95.1	98.3	93.1	99.0	96.5
8	99.3	97.2	99.7	97.2	99.3	98.3	99.3	97.9
12	99.7	97.9	99.0	96.5	100	98.3	99.7	98.3
16	100	98.6	98.3	96.5	100	97.6	99.7	98.6
20	99.7	97.9	98.7	95.8	100	96.5	99.7	99.0
Average	**99.6**	**96.9**	**98.9**	**96.2**	**99.5**	**96.8**	**99.5**	**98.1**

TABLE 3 Correct Classification Rates of Computer-Generated (CG) and Hand-Drawn (HD) Shapes Using Clamped-Plate Features

	F_1		F_2		F_3		F_4	
N	CG	HD	CG	HD	CG	HD	CG	HD
4	93.3	90.3	94.0	76.4	93.7	89.6	95.7	92.7
8	95.7	87.5	96.0	91.7	95.3	90.3	96.3	91.7
12	97.7	89.6	97.0	92.0	96.0	89.6	96.0	93.8
16	98.3	92.4	98.3	80.9	98.0	89.6	98.7	92.4
20	98.0	90.3	98.7	84.0	99.0	91.3	97.3	95.1
Average	**96.6**	**90.0**	**96.8**	**85.0**	**96.4**	**90.1**	**96.8**	**93.1**

TABLE 4 Classification Rates of Computer-Generated (CG) and Hand-Drawn (HD) Shapes Using Buckling Plate Features

	F_1		F_2		F_3		F_4	
N	CG	HD	CG	HD	CG	HD	CG	HD
4	98.0	91.3	92.7	86.8	92.7	87.8	93.7	92.7
8	93.7	91.7	94.7	89.9	93.7	87.2	93.3	90.3
12	94.7	90.3	94.0	85.8	96.0	91.3	95.0	95.8
16	94.3	92.4	95.3	89.6	96.7	92.4	96.0	95.1
20	97.7	94.4	94.7	85.4	95.7	94.1	96.0	94.1
Average	**95.7**	**92.0**	**94.3**	**87.5**	**95.0**	**90.6**	**94.8**	**93.6**

On average, the Dirichlet and the Neumann features performed comparably to each other and were consistently better than the clamped plate or the buckling plate features. The performance similarity of the Dirichlet and Neumann features was observed in some of our earlier published work (Khabou et al., 2007a,b, 2008). However, the better performance of the Dirichlet and Neumann features compared with the clamped

plate and buckling plate features is a new observation and merits further scrutiny. From an engineering perspective, this relates to the fact that the clamped plate and buckling features are based on fourth-order derivatives, whereas Dirichlet and Neumann are based on second-order derivatives, which are less sensitive to noise than the fourth order.

It is also interesting to notice that, on average, the F_1, F_3, and F_4 features seem to have similar performance, better than that of the F_2 features regardless of which Laplacian the eigenvalues are based on. This trend was also observed in some of our previously published work (Rhouma et al., 2009). We believe that this may be explained by the fact that some shapes may have completely different eigenvalues but similar multiplicity, which yields similar F_2 features. For example, if the first 5 eigenvalues of a shape S_1 are $\{2, 3, 3, 6, 6\}$ and those of a second shape S_2 are $\{1, 8, 8, 16, 16\}$, their F_2 features will be $\{2/3, 1, 1/2, 1\}$ and $\{1/8, 1, 1/2, 1\}$, respectively, which are quite similar (they differ by only one value). However, the F_1, F_3, and F_4 features, on the other hand, would be very different (for example, the F_1 features would be $\{2/3, 2/3, 1/3, 1/3\}$ and $\{1/8, 1/8, 1/16, 1/16\}$ respectively). In fact, as we argued earlier, the values of λ_{k+1}/λ_k converges to 1 as $k \to \infty$ and thus do not carry much information about a specific shape. Moreover, if two shapes Ω_1 and Ω_2 have identical eigenvalues save for the first one, then the F_2 feature vectors of both shapes are almost identical. In contrast, the feature vectors F_1, F_3, and F_4 do carry in each entry the value of λ_1, and, by Weyl's asymptotic formula, geometric content as well, even when the dimension of the feature vector is high (see Osting, 2010; Weyl, 1911).

9.3. Natural Shapes

In this experiment, we wanted to gauge and compare the performance of our features using a subset of a standard database of natural shapes. Our dataset consists of 195 images of sting ray, snapper, eel, mullet, and flounder-like fish from the standard SQUID dataset[2] (University of Surrey, UK) (samples are shown in Figure 14). The data set was divided into training and testing pools consisting of 95 and 100 images, respectively. The Dirichlet, Neumann, buckling plate, and clamped plate features were generated from all the images. To illustrate the class separation capability of the different generated features, we plotted the ratios of λ_1/λ_3 versus λ_1/λ_2 for the eel, flounder, and mullet images (we did not include the other two fish classes in the plots because they made them look busy and hard to read). These plots are shown in Figures 15–16. As can clearly

[2] See http://www.ee.surrey.ac.uk/CVSSP/demos/css/demo.html

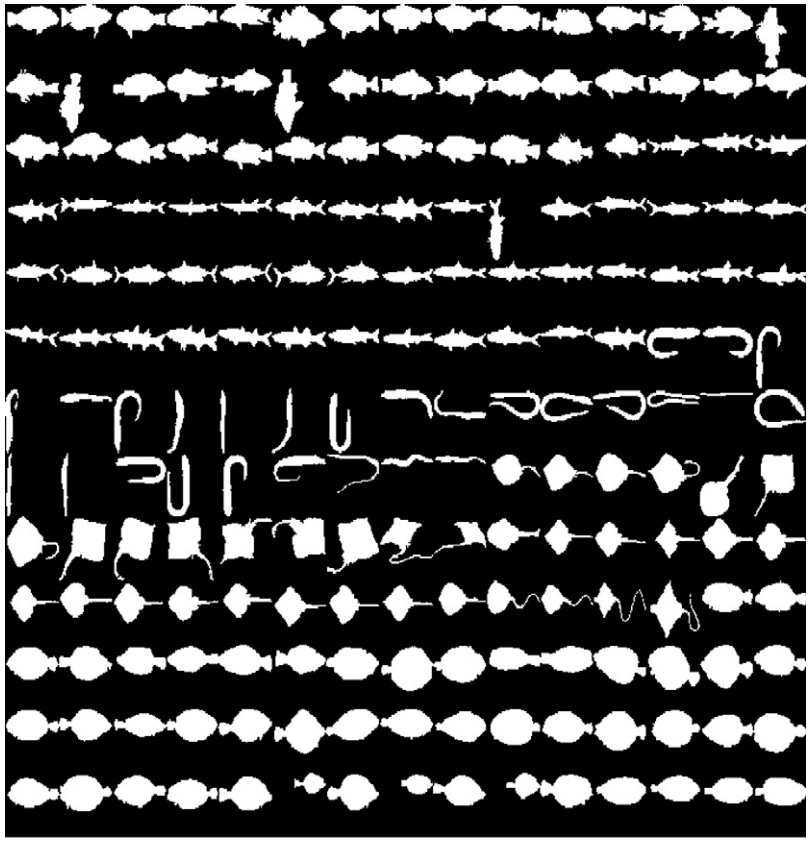

FIGURE 14 Fish images in the dataset.

be seen in these graphs, features from the same fish class seem to cluster together, exhibiting behavior similar to that described by Antunes and Henrot (2011). This clustering phenomenon is a good indication of the features' potential class separability capability. It is also worth noting that since the flounder images are the closest shapes to a disk, the values of their λ_1/λ_3 and λ_1/λ_2 are also the closest to those of a perfect disk. The values of λ_1/λ_3 and λ_1/λ_2 for the eel images are at the other end of the spectrum (very elongated shapes), whereas those of the mullets are somewhere in between (their width/length aspect ratios is somewhere between those of the flounders and the eels).

After generating the different features for all the fish images, we created simple feed-forward neural networks with one hidden layer and an input layer that uses $n = 4, 8, 12, 16$, and 20 features. These neural networks were trained using the 95 fish images in the training subset and

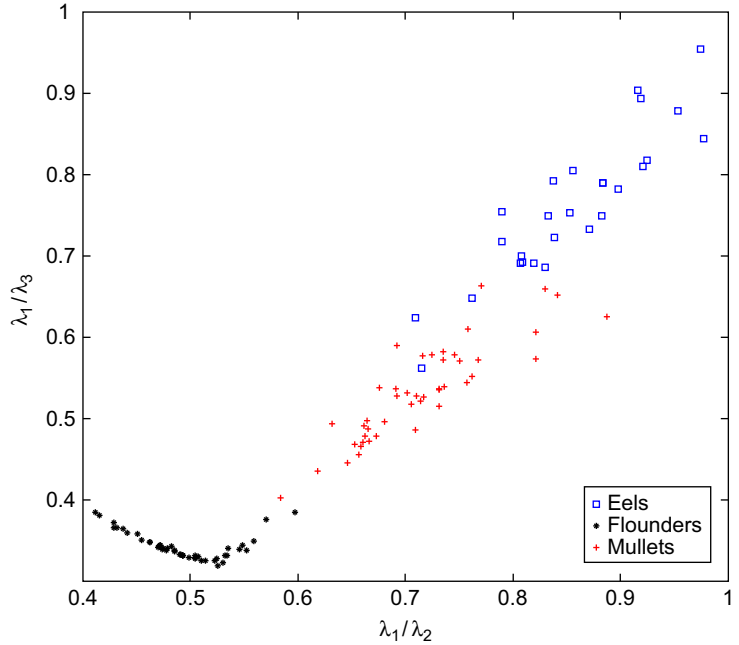

(a) Dirichlet

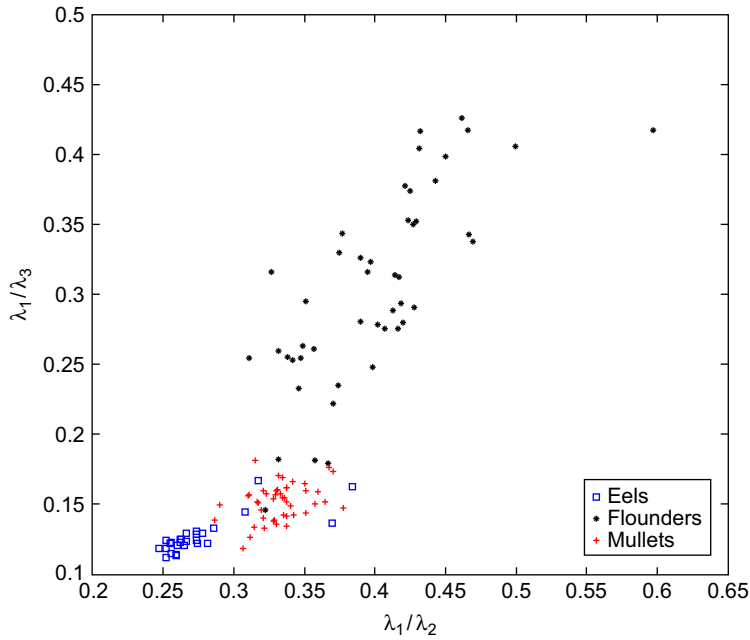

(b) Neumann

FIGURE 15 Dirichlet and Neumann λ_1/λ_3 versus λ_1/λ_2 values for eel, flounder, and mullet images.

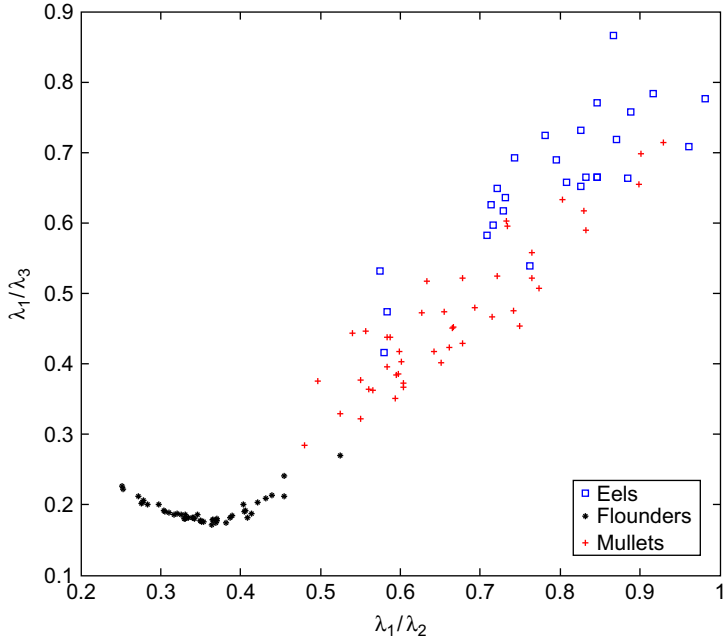

(a) Clamped

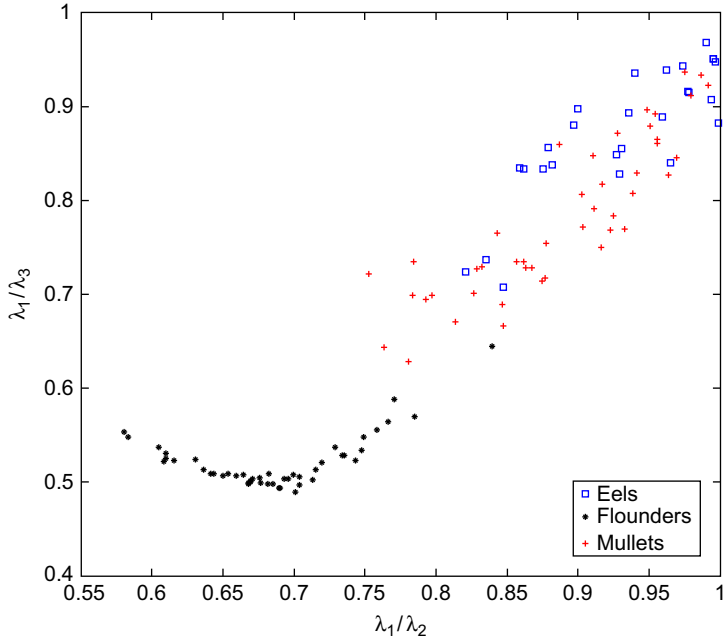

(b) Buckling

FIGURE 16 Clamped and buckling λ_1/λ_3 versus λ_1/λ_2 values for eel, flounder, and mullet images.

TABLE 5 Correct Classification Rates of the Fish Images

	Neumann				Dirichlet				Buckling-plate				Clamped-plate			
N	F_1	F_2	F_3	F_4	F_1	F_2	F_3	F_4	F_1	F_2	F_3	F_4	F_1	F_2	F_3	F_4
4	88	85	89	87	92	95	94	94	87	84	93	85	90	87	92	89
8	94	89	91	91	93	94	94	94	89	83	92	90	90	86	91	90
12	91	86	90	92	93	93	94	97	88	84	93	90	92	80	93	96
16	95	87	95	96	94	91	92	98	91	85	92	92	92	85	93	94
20	95	88	95	97	94	88	93	98	92	87	93	93	92	81	92	94
Average	**93**	**87**	**92**	**93**	**93**	**92**	**93**	**96**	**89**	**85**	**93**	**90**	**91**	**84**	**92**	**93**

tested using the 100 images in the testing subset. Table 5 shows the correct classification rates on the testing set. As clearly seen in this table, very good classification rates (above 90%) were achieved using all the feature sets, which reiterates that they are good shape discriminators and are tolerant of boundary deformation given all the variability in the fish images. It is worth mentioning that most classification errors were due to confusion between flounder-like and snapper-like images, which are the most similar classes. We also notice that, yet again, the Dirichlet and Neumann features performed similarly and better than the clamped plate and the buckling plate features. The Dirichlet and Neumann features attained better classification rates with fewer features. This shows that they are more stable and more tolerant of boundary variations. Similar to the trend observed in the computer and hand-drawn images, the clamped plate and buckling plate features had similar performance with the fish images. Also, we observe again that the F_2 features did not perform as well as the F_1, F_3, and F_4 features regardless of which eigenvalue problem is used to generate the features. On average, the Dirichlet features have an advantage over all other operators, especially when the number of features is small (see Table 5).

9.4. Effect of Holes and Boundary Noise on Features

The effect of holes and boundary deformation on the value of eigenvalues are commonly studied problems in mathematics (see, e.g., Flucher, 1995; Harrell, Kroger, & Kurata, 2001; Cox, 1995). For instance, the classical paper of Kac (1966) provides a means of extracting the number of holes contained in a domain from knowing the spectrum for a domain when its boundary is smooth.

In this set of experiments, we wanted to see how our features would react to the presence of holes of different sizes in an image and to the presence of intruding and extruding noise on the boundary. We conducted two experiments: In the first experiment, we created a sequence of square

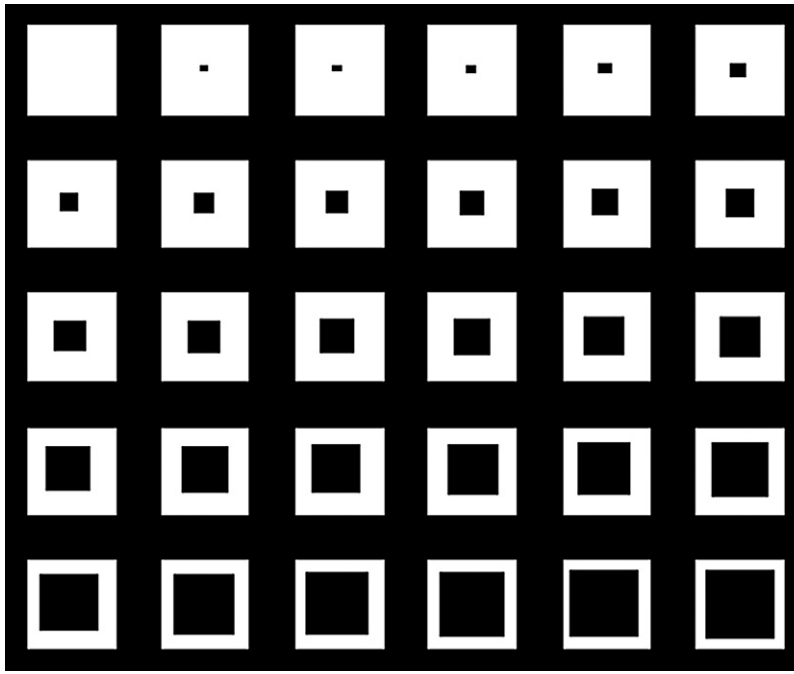

FIGURE 17 Images of squares with holes of size ranging from 0% to almost 60%.

shapes with a hole of gradually increasing size ranging from 0% to almost 55% of the solid square area (Figure 17).

We computed the first five F_1, F_2, F_3, and F_4 Neumann, Dirichlet, clamped plate, and buckling plate features of these shapes. The average and standard deviation of the feature values are plotted in Figures 18–20. The standard deviation is a measure of how the feature values varied as the size of the hole increased. Based on these graphs, it seems that the Neumann and the buckling plate features are the most tolerant of the presence of a central hole in the square shape. They exhibited the least amount of variation as the hole was introduced into the shape and its size increased. The Dirichlet and clamped plate features appear to behave similar to each other (similar standard deviation), but seem less tolerant of the holes than the Neumann and the buckling plate features. To further test these observations, we plotted the values of λ_1/λ_2 and λ_1/λ_3 as a function of the size of the central hole in Figure 20. In Figure 20a all eigenvalue ratios except the Neumann reacted to the introduction of the central hole. Since all the figures considered are symmetric, $\mu_2 = \mu_3$, resulting in a constant line at 1 in the Neumann case. To avoid multiplicity considerations as a result of symmetry, the graphs in Figure 20b clearly display the reaction of λ_3/λ_1

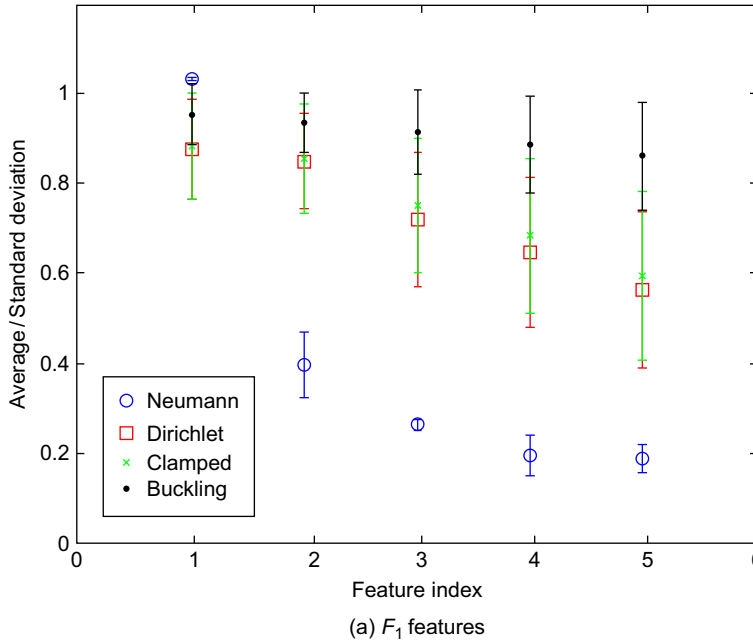

(a) F_1 features

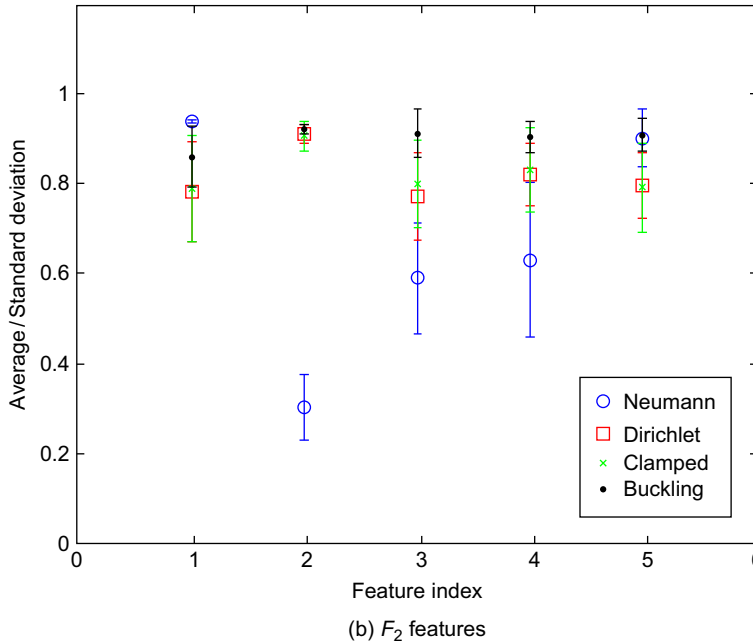

(b) F_2 features

FIGURE 18 Average and standard deviation of the first five features for Neumann, Dirichlet, clamped, and buckling problems.

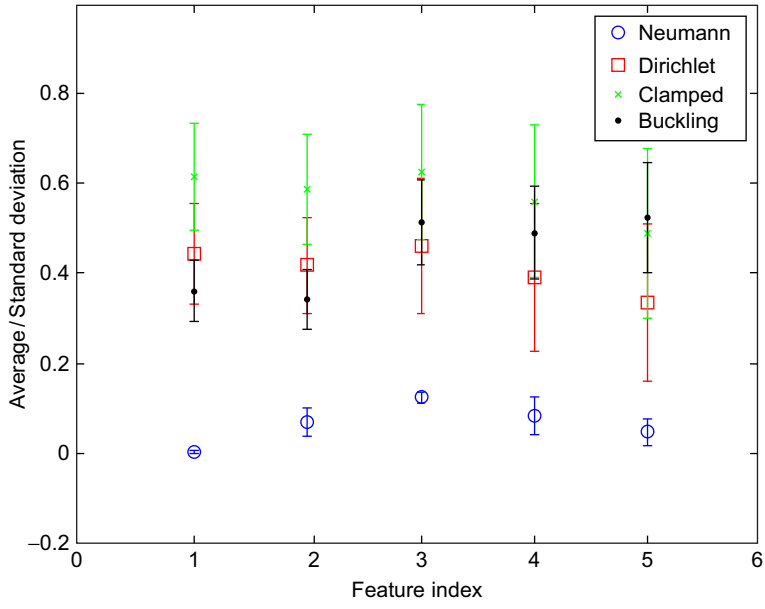

(a) F_3 features

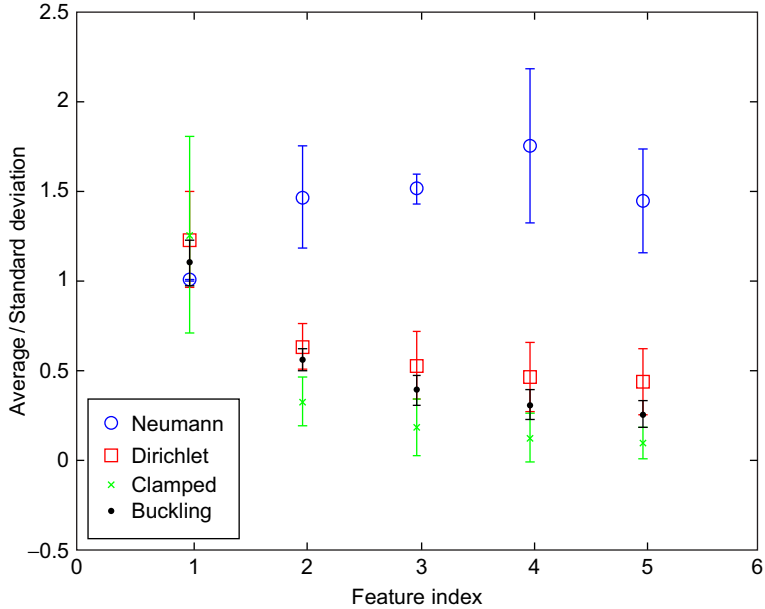

(b) F_4 features

FIGURE 19 Average and standard deviation of the first five features for Neumann, Dirichlet, clamped, and buckling problems.

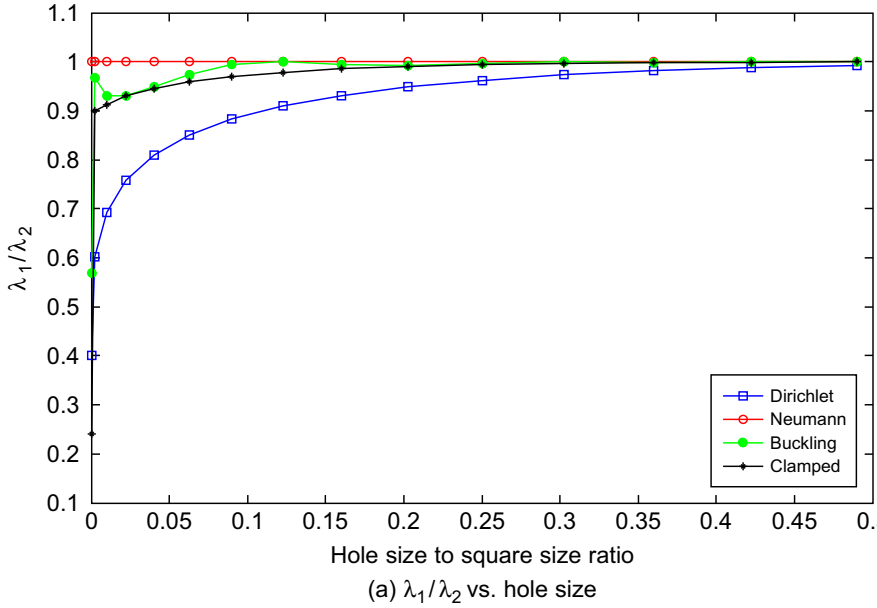

(a) λ_1/λ_2 vs. hole size

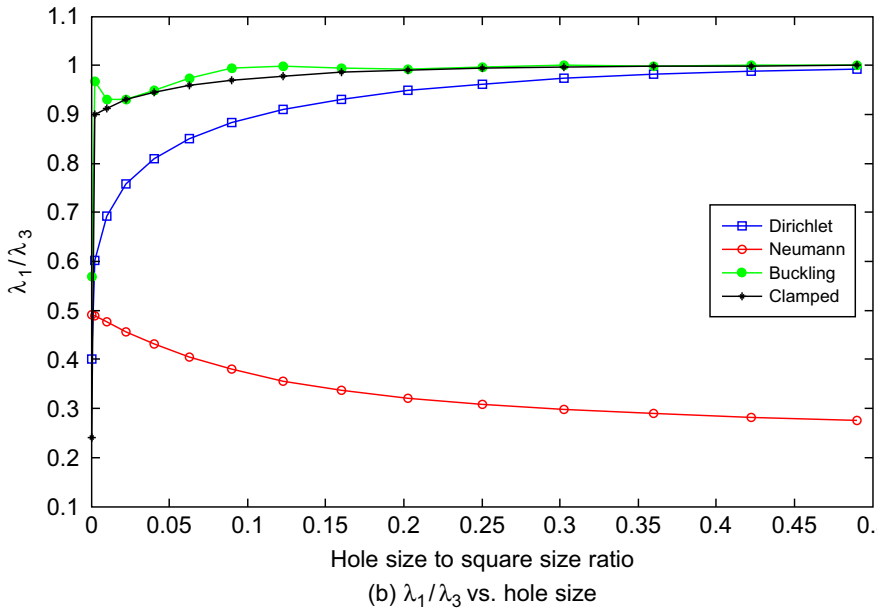

(b) λ_1/λ_3 vs. hole size

FIGURE 20 λ_1/λ_2 and λ_1/λ_3 as a function of hole size for various operators.

to the gradual increase of the hole size. As the domain thins, all graphs in Figures 20a and b exhibit a clearly defined asymptotic behavior that translates into an inability to "hear domains with large holes" for features built of ratios of eigenvalues.

In the second experiment, we wanted to investigate the effect of multiple holes and the presence of intruding and extruding boundary noise on the feature values. We created 12 square and 12 disk shapes with various extruding and intruding "noise" and/or different numbers of holes in them (Figures 21a and b). We then computed their Neumann, Dirichlet, clamped plate, and buckling plate eigenvalues. We plotted the ratios of λ_1/λ_2, λ_1/λ_3, and λ_1/λ_4, in Figures 22–24. All features reacted to the "noise" and hole(s) to some degree. All features seemed to react the most to the intruding "noise" in image 6 (row 2, column 2). The reaction to the hole(s) seemed less pronounced than the reaction to the intruding or extruding noise. Overall, the Dirichlet features seemed to react relatively the least to the "noise."

10. CONCLUSION

Eigenvalues of Laplacian operators were used to create translation-, rotation-, and size-invariant features for shape description and recognition purposes. Sets of experiments conducted with simple shapes show that the features confirm a set of known theoretical properties discussed in details in this chapter. Also, we observe that the features exhibit some interesting asymptotic behaviors. The features were also used to classify computer-generated, hand-drawn, and natural images with a great level of accuracy. The excellent classification results, which were achieved using a relatively small number of features (only four features in some cases), demonstrate that these features have a good interclass discrimination capability and can successfully be used to greatly compress the information necessary to represent and index a particular shape (e.g., in a searchable shape database). The Dirichlet and Neumann features performed almost identically in our classification tests as did the clamped plate and buckling plate features. We noticed that the Dirichlet and Neumann features had a consistent slight edge in performance compared with the clamped plate and buckling plate features.

The stability of all features in the presence of noise, boundary deformation, and holes was investigated. All features proved quite stable and tolerant of noise, small boundary deformation, and small holes. This indicates that these features, in essence, capture the dominant (i.e., low-pass filtered) portion of the shape and are not very sensitive to small variations on a shape's boundary.

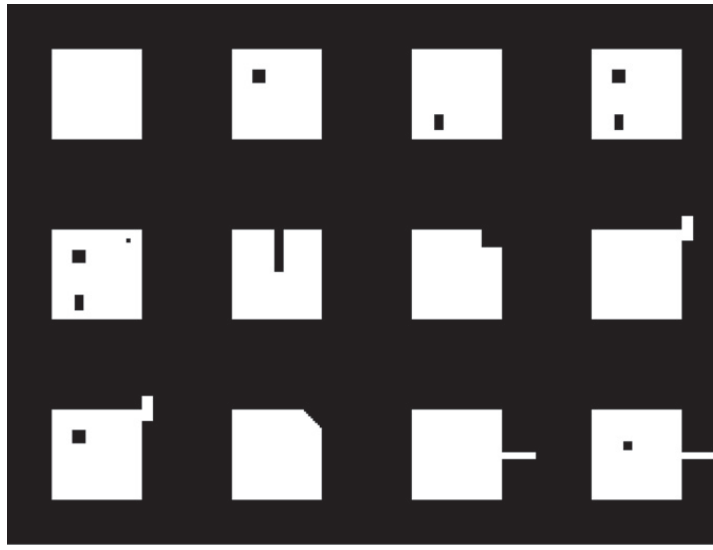

(a) Twelve square shapes with various types of "noise."

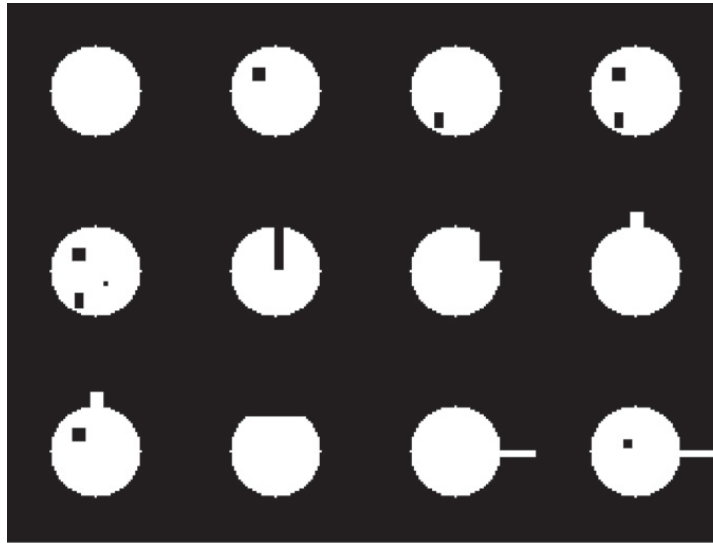

(b) Twelve disk shapes with various types of "noise."

FIGURE 21 Aberrations of basic shapes via hole and boundary "noise."

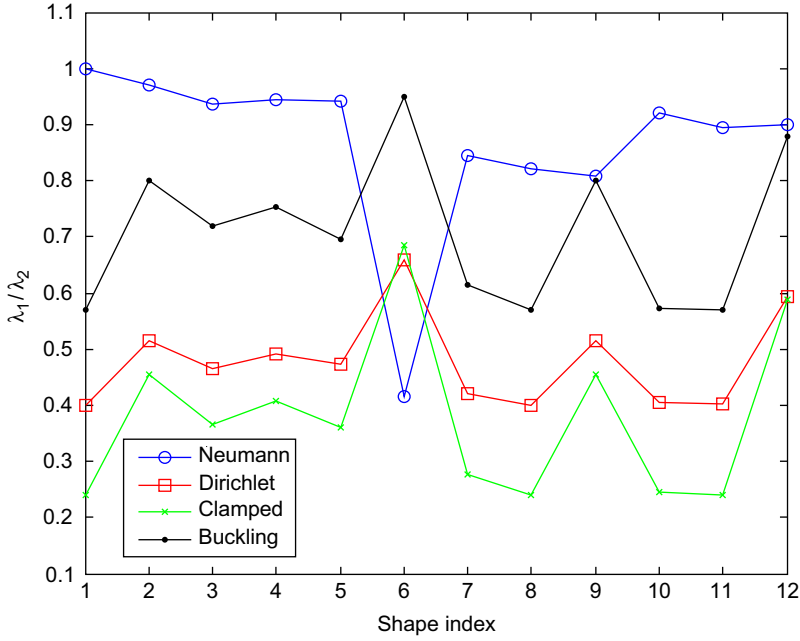

(a) λ_1 / λ_2 values of the 12 square shapes

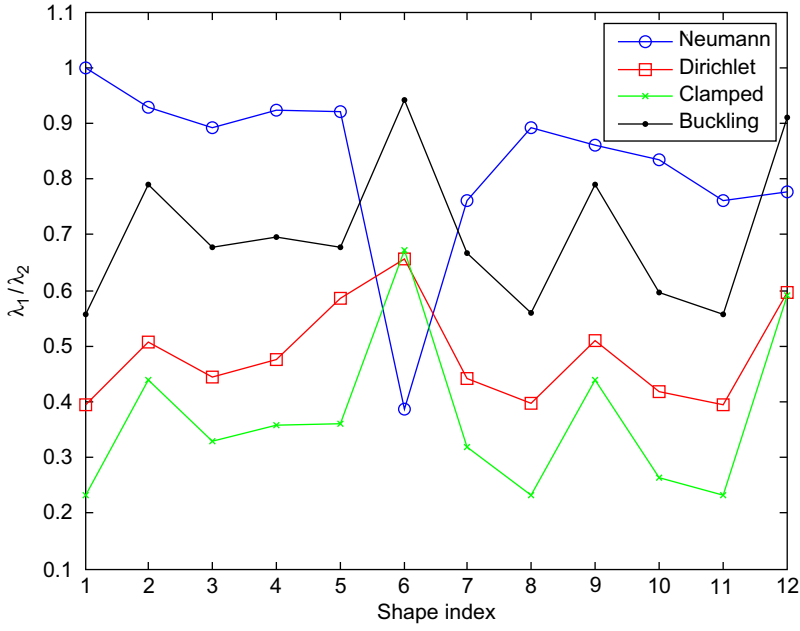

(b) λ_1 / λ_2 values of the 12 disk shapes

FIGURE 22 Effect of "noise" on λ_1/λ_2.

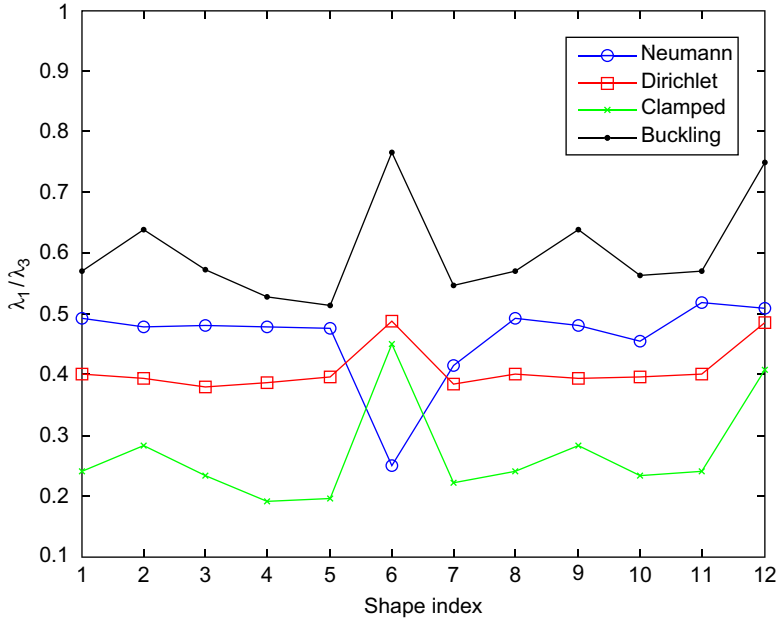

(a) λ_1/λ_3 values of the 12 square shapes

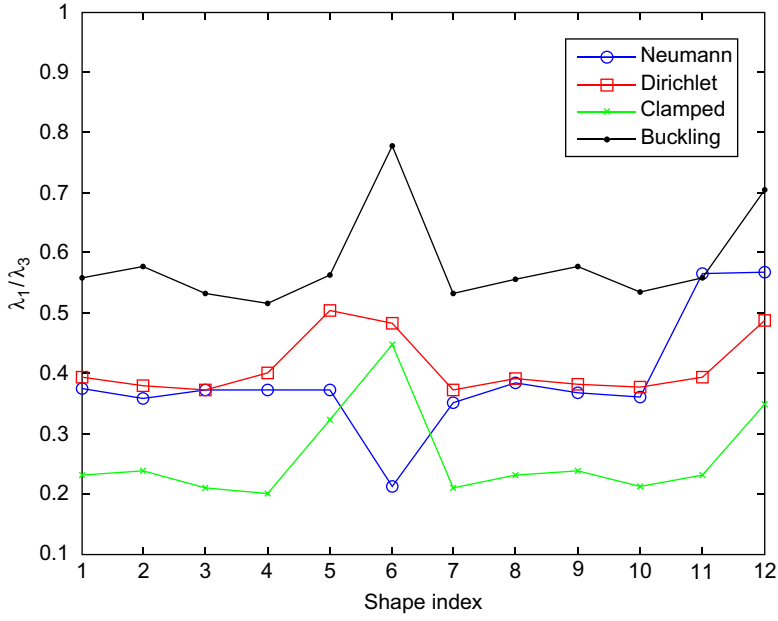

(b) λ_1/λ_3 values of the 12 disk shapes

FIGURE 23 Effect of "noise" on λ_1/λ_3.

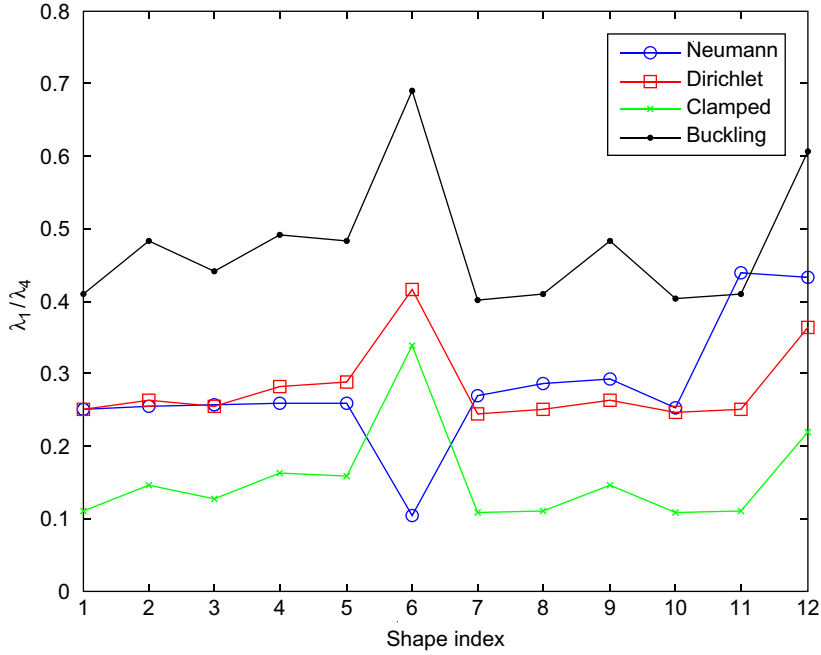

(a) λ_1/λ_4 values of the 12 square shapes

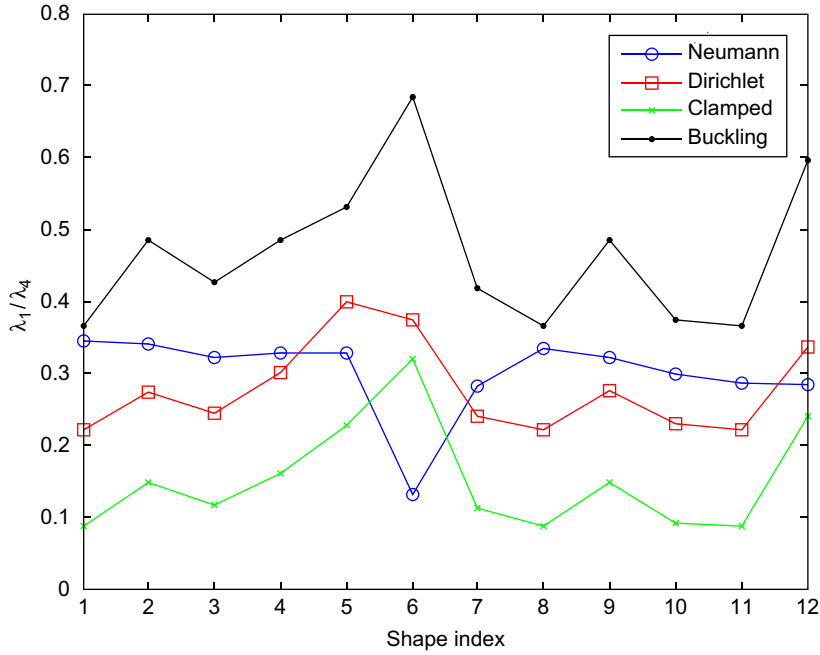

(b) λ_1/λ_4 values of the 12 disk shapes

FIGURE 24 Effect of "noise" on λ_1/λ_4.

ACKNOWLEDGMENTS

The authors thank Dr. Peter Hawkes for his patience and kindness while writing this paper. Part of this work was presented by Lotfi Hermi as a mini-course for the Swiss Doctoral Program, "Shape Recognition Schemes Based on the Spectrum of the Laplacian," University of Neuchâtel, June 8–12, 2009. We thank Professor Bruno Colbois and the University of Neuchâtel for their hospitality and generosity. We recognize internal financial support for Mohamed Ben Haj Rhouma by Sultan Qaboos University and support for Lotfi Hermi by the Erwin Schrödinger Institute, while performing this work.

REFERENCES

Aimi, A., & Diligenti, M. (1992). Difetti ed eccessi degli autovalori del classico problema di "buckling" (Upper and lower bounds of eigenvalues of the classical buckling problem). *Calcolo, 29*, 313–328.

Aimi, A., & Diligenti, M. (1994). Stima dell'errore nel calcolo degli autovettori nel problema del "buckling" di una piastra incastrata al bordo (Error estimation in the computation of eigen-vectors in the buckling problem for a plate embedded at the boundary). *Calcolo*, *30*(1993), 171–187.

Antunes, P., & Freitas, P. (2006). New bounds for the principal Dirichlet eigenvalue of planar regions. *Experimental Mathematics, 15*, 333–342.

Antunes, P., & Henrot, A. (2011). On the range of the first two Dirichlet and Neumann eigenvalues of the Laplacian. *Proceedings of the Royal Society London Series A (Mathematical Physical Engineering Science)* (Vol. 467) (pp. 1577–1603).

Arbter, K. (1989). Affine-invariant Fourier descriptors. In J. C. Simon (Ed.), *From pixels to features* (pp. 153–164). North-Holland: Elsevier Science.

Ashbaugh, M. S. (1999a). Isoperimetric and universal inequalities for eigenvalues. In E. B. Davies & Y. Safarov (Eds.), *Spectral theory and geometry (London Mathematical Society Lecture Notes)* (Vol. 273) (pp. 95–139). Cambridge: Cambridge University Press.

Ashbaugh, M. S. (1999b). Open problems on eigenvalues of the Laplacian. In T. M. Rassias & H. M. Srivastava (Eds.), *Analytic and geometric inequalities and applications, mathematcs with applications* (vol. 478) (pp. 13–28). Dordrecht: Kluwer Academic.

Ashbaugh, M. S. (2002). The universal eigenvalue bounds of Payne-Polya-Weinberger. In H. Protter & H. C. Yang (Eds.), *Proceedings of the Indian academy of sciences (Mathematical science)* (vol. 112) (pp. 3–30). Heidelberger: Springer Verlag.

Ashbaugh, M. S. (2004). On universal inequalities for the low eigenvalues of the buckling problem. In C. Conca, R. Manásevich, G. Uhlmann, & M. S. Vogelius (Eds.), *Partial differential equations and inverse problems, contemporary mathematics* (vol. 362) (pp. 13–31). Providence, RI: American Mathematical Society.

Ashbaugh, M. S., & Benguria, R. D. (1991). Proof of the Payne-Polya-Weinberger conjecture. *Bulletin of the American Meteorological Society, 25*, 19–29.

Ashbaugh, M. S., & Benguria, R. D. (1992). A sharp bound for the ratio of the first two eigenvalues of Dirichlet Laplacians and extensions. *Annals Mathematics, 135*, 601–628.

Ashbaugh, M .S., & Benguria, R. D. (1993a). Isoperimetric inequalities for higher eigenvalue ratios for the n-dimensional fixed membrane problem. *Proceedings of the Royal Society Edinburgh A, 123*, 977–985.

Ashbaugh, M. S., & Benguria, R. D. (1993b). More bounds on eigenvalue ratios for Dirichlet Laplacians in nn dimensions. *SIAM Journal on Mathematical Analysis, 24*, 1622–1651.

Ashbaugh, M. S., & Benguria, R. D. (1993c). Universal bounds for the low eigenvalues of Neumann Laplacians in n dimensions. *SIAM Journal on Mathematical Analysis, 24*, 557–570.

Ashbaugh, M. S., & Benguria, R. D. (1994a). Bounds for ratios of eigenvalues of the Dirichlet Laplacian. *Proceedings of the American Mathematical Society, 121*, 145–150.

Ashbaugh, M. S., & Benguria, R. D. (1994b). The range of values of λ_2/λ_1 and λ_3/λ_1 for the fixed membrane problem. The state of matter (Copenhagen, 1992). *Advanced Series Mathematical Physics, 20*, 167–181.

Ashbaugh, M. S., & Benguria, R. D. (1994c). The range of values of λ_2/λ_1 and λ_3/λ_1 for the fixed membrane problem. Special issue dedicated to Elliott H. Lieb. *Reviews in Mathematical Physics, 6*, 999–1009.

Ashbaugh, M .S., & Benguria, R. D. (1995). On Rayleigh's conjecture for the clamped plate and its generalization to three dimensions. *Duke Mathematics Journal, 78*, 1–17.

Ashbaugh, M. S., & Benguria, R. D. (2007). Isoperimetric inequalities for eigenvalues of the Laplacian. In F. Gesztesy, P. Deift, C. Galvez, P. Perry & W. Schlag (Eds.), *Spectral theory and mathematical physics: A festschrift in honor of barry simon's 60th birthday (Proceedings of the symposium on pure mathematics 76, part 1)* (pp. 105–139). Providence, RI: American Mathematical Society.

Ashbaugh, M. S., Benguria, R. D., & Laugesen, R. S. (1997). Inequalities for the first eigenvalues of the clamped plate and buckling problems. *International Series of Numerical Mathematics, 123*, 95–110.

Ashbaugh, M. S., Gesztesy, F., Mitrea, M., Shterenberg, R., & Teschl, G. (2010). The Krein-von Neumann extension and its connection to an abstract buckling problem. *Mathematical Nachrichten, 283*, 165–179.

Ashbaugh, M. S., & Hermi, L. (2008). On extending the inequalities of Payne, Polya, and Weinberger using spherical harmonics. *Rocky Mountain Journal of Mathematics, 38*, 1037–1072.

Ashbaugh, M. S., & Laugesen, R. S. (1996). Fundamental tones and buckling loads of clamped plates. *Annali Scuola Normale Superiore Pisa Classe Scienze, 23*, 383–402.

Barnett, A. H. (2009). Perturbative analysis of the method of particular solutions for improved inclusion of high-lying Dirichlet eigenvalues. *SIAM Journal on Numerical Analysis, 47*, 1952–1970.

Belkin, M., & Niyogi, P. (2003). Laplacian eigenmaps for dimensionality reduction and data representation. *Neural Computing, 15*, 1373–1396.

Benguria, R. D., & Linde, H. (2008). Isoperimetric inequalities for eigenvalues of the Laplace operator. In C. Villegas-Blas (Ed.), *Fourth summer school in analysis and mathematical physics, 140, contemporary mathematical* (vol. 476) (pp. 1–40). Providence, RI: American Mathematical Society.

Berretti, S., Bimbo, A. D., & Pala, P. (2000). Retrieval by shape similarity with perceptual distance and effective indexing. *IEEE Transactions Multimedia, 2*, 225–239.

Betcke, T., & Trefethen, L. N. (2005). Reviving the method of particular solutions. *SIAM Review, 47*, 469–491.

Blum, H. (1967). A transformation for extracting new descriptors of shape. In W. Whaten-Dunn (Ed.), *Models for the perception of speech and visual forms* (pp. 362–380). Cambridge, MA: MIT Press.

Bramble, J. H., & Hubbard, B. E. (1968). Effects of boundary regularity on the discretization error in the fixed membrane eigenvalue problem. *SIAM Journal of Numerical Analysis, 5*, 835–863.

Bramble, J. H., & Payne, L. E. (1963). Pointwise bounds in the first biharmonic boundary value problem. *Journal of Mathematics and Physics, 42*, 278–286.

Burden, R. L., & Hedstrom, G. W. (1972). The distribution of the eigenvalues of the discrete Laplacian. *Nordisk Tidskrift Informationsbehandling (BIT), 12*, 475–488.

Buser, P., Conway, J., Doyle, P., & Semmler, K. D. (1994). Some planar isospectral domains. *International Mathematics Research Notices, 391*, 9.

Chellappa, R., & Bagdazian, R. (1984). Fourier coding of image boundaries. *IEEE Transactions on Pattern Analysis and Machine Intelligence, 6*, 102–105.

Chen, D., & Zheng, T. (2011). Bounds for ratios of membranes eigenvalues. *Journal of Differentiation Equations, 250*, 1575–1590.

Cheng, Q.-M., & Yang, H. C. (2006a). Inequalities for eigenvalues of a clamped plate problem. *Transactions on American Mathematical Society, 358*, 2625–2635.

Cheng, Q.-M., & Yang, H. C. (2006b). Universal bounds for eigenvalues of a buckling problem. *Communications in Mathematical Physics, 262*, 663–675.

Cheng, Q. M., & Yang, H. C. (2007). Bounds on eigenvalues of Dirichlet Laplacian. *Mathematical Annals, 337*, 159–175.

Chomsky, N. (1957). *Syntactic structures.* The Hague, Berlin: Mouton.

Coifman, R. R., Kevrekidis, I. G., Lafon, S., Maggioni, M., & Nadler, B. (2008). Diffusion maps, reduction coordinates and low dimensional representation of stochastic systems. *SIAM Multiscale Modeling and Simulation, 7*, 842–864.

Courant, R., & Hilbert, D. (1953). *Methods of mathematical physics* (vol. I). New York: InterScience Publishing.

Cox, S. J., & Ross, M. (1995). Extremal eigenvalue problems for starlike planar domains. *Journal of differential Equations, 120*, 174–197.

Davies, E. R. (1997). *Machine vision: Theory, algorithms, practicalities* (pp. 171–191). New York: Academic Press.

Driscoll, T. A. (1997). Eigenmodes of isospectral drums. *SIAM Review, 39*, 1–17.

Fichera, G. (1967). Structure of Green's operators and estimates for the corresponding eigenvalues. In V. Seda (Ed.), *Differential equations and their applications* (Proceedings of the Conference held in Bratislava in September 1966, Slovenske pedagogicke nakladatel'stvo, Bratislava, 1967) (pp. 249–272). Bratislava, Czechoslovakia: Comenius University.

Flucher, M. (1995). Approximation of Dirichlet eigenvalues on domains with small holes. *Journal of Mathematical Analysis and Applications, 193*, 169–199.

Flussera, J., & Suka, T. (1993). Pattern recognition by affine moment invariants. *Pattern Recognition, 26*, 167–174.

Forsythe, G. E. (1954). Asymptotic lower bounds for the frequencies of certain polygonal membranes. *Pacific Journal of Mathematics, 4*, 467–480.

Forsythe, G. E. (1955). Asymptotic lower bounds for the fundamental frequency of convex membranes. *Journal of Mathematics, 5*, 691–702.

Forsythe, G. E., & Wasow, W. R. (2004). *Finite-difference methods for partial differential equations*. (Reprint of the 1960 original.) Dover Phoenix Editions. Mineola, New York: Dover Publications.

Fox, L., Henrici, P., & Moler, C. (1967). Approximations and bounds for eigenvalues of elliptic operators. *SIAM Journal on Numerical Analysis, 4*, 89–102.

Friedlander, L. (1991). Some inequalities between Dirichlet and Neumann eigenvalues. *Archive for Rational Mechanics and Analysis, 116*, 153–160.

Fu, K. S. (1974). *Syntactic methods in pattern recognition.* New York: Academic Press.

Fusco, N., Maggi, F., & Pratelli, A. (2009). Stability estimates for certain Faber-Krahn, isocapacitary and Cheeger inequalities. *Annali Scuola Normale Superiore Pisa Classe Science, 8*, 51–71.

Gordon, C., Webb, D., & Wolpert, S. (1992). One cannot hear the shape of a drum. *Bulletin of the American Mathematical Society, 27*, 134–138.

Girouard, A., & Polterovich, I. (2010). Shape optimization for low Neumann and Steklov eigenvalues. (Special issue on Complex-Analytic Methods). *Mathematical Methods in Applied Science, 33*, 501–516.

Grinspun, E., Kälberer, F., Mathur, S., & Wardetzky, M. (2007). Discrete Laplace operators: No free lunch. ACM International Conference Proceeding Series 257 (2007), *Proceedings of the fifth eurographics symposium on geometry processing, Barcelona, Spain* (pp. 33–37).

Groskey, W. I., & Mehrotra, R. (1990). Index-based object recognition in pictorial data management. *Computational Vision Graphics Image Process., 52*, 416–436.

Groskey, W. I., Neo, P., and Mehrotra, R. A. (1992). A pictorial index mechanism for model-based matching. *Data Knowledge Engineering, 8*, 309–327.

Guidotti, P., & Lambers, J. V. (2008). Eigenvalue characterization and computation for the Laplacian on general 2-D domains. *Numerical Functional Analysis Optimization, 29*, 507–531.

Harrell, E. M., & Hermi, L. (2008). Differential inequalities for Riesz means and Weyl-type bounds for eigenvalues. *Journal of Functional Analysis, 254*, 3173–3191.

Harrell, E. M., & Hermi, L. (2008). On Riesz means of eigenvalues. Preprint 2008, *Computational Particle Differential Equations* (forthcoming). Accepted for Publication in Communications in Partial Differential Equations.

Harrell, E. M., Kroger, P., & Kurata, K. (2001). On the placement of an obstacle or a well so as to optimize the fundamental eigenvalue. *SIAM Journal on Mathematical Analysis, 33*, 240–259.

Harrell, E. M., & Stubbe, J. Trace identities for commutators, with applications to the distribution of eigenvalues. *Transactions of the American Mathematical Society* (forthcoming); available as arXiv:/0903.0563.

Harrell, E. M., & Stubbe, J. (1997). On trace identities and universal eigenvalue estimates for some partial differential operators. *Transactions of the American Mathematical Society, 349*, 1797–1809.

Haykin, S. (1994). *Neural networks, A comprehensive foundation*. New York: MacMillan.

Henrot, A. (2006). *Extremum problems for eigenvalues of elliptic operators. Frontiers in mathematics*. Basel: Birkhuser Verlag.

Henrot, A., & Oudet, E. (2003). Minimizing the second eigenvalue of the Laplace operator with Dirichlet boundary conditions. *Archive for Rational Mechanics and Analysis, 169*, 73–87.

Hermi, L. (2008). Two new Weyl-type bounds for the Dirichlet Laplacian. *Transactions of the American Mathematical Society, 360*, 1539–1558.

Hile, G. N., & Protter, M. H. (1980). Inequalities for eigenvalues of the Laplacian. *Indiana University Mathematics Journal, 29*, 523–538.

Hile, G. N., & Yeh, R. Z. (1984). Inequalities for eigenvalues of the biharmonic operator. *Pacific Journal of Mathematics, 112*, 115–133.

Hornik, K., Stinchrombe, M., & White, H. (1990). Universal approximation of an unknown mapping and its derivatives using multilayer feed-forward networks. *Neural Networks, 3*, 551–560.

Hu, M. K. (1962). Visual pattern recognition by moment invariants. *IRE Transactions on Information Theory, IT-8*, 179–187.

Hubbard, B. (1961). Bounds for eigenvalues of the free and fixed membrane by finite difference methods. *Pacific Journal of Mathematics, 11*, 559–590.

Iivarinen, J., & Visa, A. (1996). Shape recognition of irregular objects. In D. P. Casasent (Ed.), *Intelligent robots and computer vision XV: Algorithms, techniques, active vision, and materials handling, Proceedings of SPIE 2904* (pp. 25–32). SPIE (Society of Photo-Optical Instrumentation Engineers), Belligham, WA.

Jones, P. W., Maggioni, M., & Schul, R. (2008). Manifold parametrizations by eigenfunctions of the Laplacian and heat kernels. *Proceedings of the National Academy of Sciences, 105*, 1803–1808.

Kac, M. (1966). Can one hear the shape of a drum? *American Mathematical Monthly, 73*, 1–23.

Keller, H. B. (1965). On the accuracy of finite difference approximations to the eigenvalues of differential and integral operators. *Numerical Mathematics, 7*, 412–419.

Khabou, M. A., Hermi, L., & Rhouma, M. B. H. (2007a). Shape recognition using the eigenvalues of the Dirichlet Laplacian. *Pattern Recognition, 40*, 141–153.

Khabou, M. A., Rhouma, M. B. H., & Hermi, L. (2007b). Feature generation using the Laplacian operator with Neumann boundary condition. In *Proceedings of the IEEE southeast conference* (pp. 766–771). IEEE, Piscataway, NJ.

Khabou, M. A., Rhouma, M. B. H., & Hermi, L. (2008). Performance comparison of Laplacian-based features. In *Proceedings of the international conference on image processing, computer vision, and pattern recognition*. CSREA Press, Athens.

Khotanzad, A., & Hong, Y. H. (1990). Invariant image recognition by Zernike moments. *IEEE Transactions on Pattern Analysis and Machine Intelligence, 12*, 489–497.

Kim, W. Y., & Kim, Y. S. (2000). A region-based shape descriptor using Zernike moments. *Signal Processes Image Communications, 16*, 95–102.

Kornhauser, E. T., & Stakgold, I. (1952). A variational theorem for $\nabla^2 u + \lambda u = 0$ and its applications. *Journal of Mathematics Physics, 31*, 45-54.

Kröger, P. (1992). Upper bounds for the Neumann eigenvalues on a bounded domain in Euclidean space. *Journal of Functional Analysis, 106*, 353–357.

Kuttler, J. R. (1970a). Finite difference approximations for eigenvalues of uniformly elliptic operators. *SIAM Journal for Numerical and Analytical, 7*, 206–232.

Kuttler, J. R. (1970b). Upper and lower bounds for eigenvalues by finite differences. *Pacific Journal of Mathematics, 35*, 429–440.

Kuttler, J. R. (1980). Finite-difference approximations for the Stekloff and membrane eigenvalue problems. *Bulletin Calcutta Mathematical Society, 72*, 49–68.

Kuttler, J. R., & Sigillito, V. G. (1984). Eigenvalues of the Laplacian in two dimensions. *SIAM Review, 26*, 163–193.

Lee, D. T. (1982). Medial axis transformation of a planar shape. *IEEE Transactions on Pattern Analysis and Machine Intelligence, 4*, 363–369.

Levitin, M., & Yagudin, R. (2003). Range of the first three eigenvalues of the planar Dirichlet Laplacian. *London Mathematical Society Journal of Computational and Mathematical, 6*, 1–17.

Loncarcic, S. (1998). A survey of shape analysis techniques. *Pattern Recognition, 31*, 983–1001.

Lyashenko, I. N., Meredov, Kh. M., & Embergenov, A. (1984). Investigation of the variational-difference method for determining the eigenvalues of the Laplace operator (Russian). *Izvestiya Akademii Nauk Turkmen SSR Series Fizika-Tekhn. Khimiya Geologica Nauk, 2*, 1016–1059.

Makai, E. (1962). On the principal frequency of a membrane and the torsional rigidity of a beam. In G. Szegö (Ed.), *Studies in mathematical analysis and related topics: Essays in honor of george polya* (pp. 227–231). Stanford, CA: Stanford University Press.

McCulloch, W., & Pitts, W. (1943). A logical calculus of ideas immanent in nervous activity. *Bulletin of Mathematical Biophysics, 5*, 115–133.

Mehrotra, R., and Gary, J. E. (1995). Similar-shape retrieval in shape data management. *IEEE Computational, 28*, 57–62.

Melas, A. D. (2003). A lower bound for sums of eigenvalues of the Laplacian. *Proceedings of the American Mathematical Society, 131*, 631–63.

Moler, C. B. (1965). Finite difference methods for the eigenvalues of Laplace's operator. Doctoral thesis, Stanford University.

Moler, C. B., & Payne, L. E. (1968). Bounds for eigenvalues and eigenvectors of symmetric operators. *SIAM Journal on Numerical Analysis, 5*, 64–70.

Moon, C. R., Mattos, L. S., Foster, B. K., Zeltzer, G., Ko, W., & Manoharan, H. C. (2008). Quantum phase extraction in isospectral electronic nanostructures. *Science, 8*, 782–787.

Ng, A.Y., Jordan, M. I., & Weiss, Y. (2002). On spectral clustering: Analysis and an algorithm. In T. Dietterich, S. Becker, & Z. Ghahramani (Eds.), *Advances in neural information*. Cambridge, MA: MIT Press.

Niblack, W., Barber, R., Equitz, W., Flickner, M., Glasman E., Petkovic, D., et al. (1993). The QBIC project: Querying image by content using color, texture and shape. In *Proceedings of*

SPIE storage and retrieval for image and video databases, (Vol. 1908, pp. 173–187). SPIE (Society of Photo-Optical Instrumentation Engineers), Belligham, WA.

Niethammer, M., Reuter, M., Wolter, F., Bouix, S., Patene, G., & Spagnuolo, M. (2007). Discrete Laplace-Beltrami operators for shape analysis and segmentation. *Lect Notes Computer Science, 10*, 850–857.

Oden, J. T. (1990). In S. G. Nash, *Historical comments on finite elements.* Originally published as *A history of scientific computing* (pp. 128–152), Association for Computing Machinery, Inc., reprinted by permission by Society for Industrial and Applied Mathematics, 2007. New York, NY.

Okada, Y., Shudo, A., Tasaki, S., & Harayama, T. (2005). Can one hear the shape of a drum? Revisited. *Journal of Physical Series A, 38*, L163–L170.

Osting, B. (2010). Optimization of spectral functions of Dirichlet-Laplacian eigenvalues. *Journal of Computational Physics, 229*, 8578–8590.

Otterloo, P. J. (1991). *A contour-oriented approach to shape analysis*. (pp. 90–108). New York: Prentice-Hall.

Payne, L. E. (1955). Inequalities for eigenvalues of membranes and plates. *Journal of Rational Mechanics and Analysis, 4*, 517–529.

Payne, L. E. (1960/1961). A note on inequalities for plate eigenvalues. *Journal of Mathematics and Physics, 39*, 155–159.

Payne, L. E. (1967). Isoperimetric inequalities and their applications. *SIAM Review, 9*, 453–488.

Payne, L. E. (1991). Some comments on the past fifty years of isoperimetric inequalities. Inequalities (Birmingham, 1987). *Lecture Notes in Pure Applied Mathematics, 129*, 143–161.

Payne, L. E., Polya, G., & Weinberger, H. F. (1956). On the ratio of consecutive eigenvalues. *Journal of Mathematics and Physics, 35*, 289–298.

Payne, L. E., & Weinberger, H. F. (1958). New bounds for solutions of second order elliptic partial differential equations. *Pacific Journal of Mathematics, 8*, 551–573.

Peinecke, N., Wolter, F., & Reuter, M. (2007). Laplace spectra as fingerprints for image recognition. *Computer Aided Design, 39*, 460–476.

Peura, M., & Iivarinen, J. (1997). Efficiency of simple shape descriptors. In *Proceedings of the third international workshop on visual form* (pp. 443–451). Italy: Capri.

Poggio, T., and Girosi, F. (1990). Networks for approximation and learning. *Processing IEEE, 78*, 1481–1497.

Pólya, G. (1952a). Remarks on the foregoing paper. *Journal of Mathematics Physics, 31*, 55–57.

Pólya, G. (1952b). Sur une interpretation de la methode des differences nies qui peut fournir des bornes superieures ou inferieures. *C R Academy Science Paris, 235*, 995–997.

Pólya, G. (1954). Estimates for eigenvalues. By Friends, Colleagues and Pupils. *Studies in mathematics and mechanics presented to richard von mises* (pp. 200–207). New York: Academic Press.

Pólya, G. (1960). Two more inequalities between physical and geometrical quantities. *Journal of Indian Mathematical Society (N.S.), 24*, 413–419.

Pólya, G., & Szegö, G. (1951). *Isoperimetric inequalities in mathematical physics*. Princeton, NJ: Princeton University Press.

Protter, M. H. (1987). Can one hear the shape of a drum? Revisited. *SIAM Review, 29*, 185–197.

Reeves, A. P., Prokop, R. J., Andrews, S. E., & Kuhl, F. P. (1988). Three-dimensional shape analysis using moments and Fourier descriptors. *IEEE Transactions Pattern Analysis and Machine Intell, 12*, 937–943.

Reuter, M. (2010). Hierarchical shape segmentation and registration via topological features of Laplace-Beltrami eigenfunctions. *International Journal of Computational Vision, 89*(2), 287–308.

Reuter, M., Biasotti, S., Giorgi, D., Peinecke, N., Koo M. S, & Shenton, M. E. (2009a). Global medical shape analysis using the Laplace-Beltrami spectrum. *Computers and Graphics, 33*, 381–390.

Reuter, M., Niethammer, M., Wolter, F., Peinecke, N., Bouix, S., & Shenton, M. E. (2007). Global medical shape analysis using the volumetric Laplace spectrum. In *Proceedings of the 2007 international conference on cyberworlds (NASAGEM).*(pp. 417–426). IEEE, Piscataway, NJ.

Reuter, M., Wolter, F., & Peinecke N. (2005a). Laplace-Beltrami as finger prints for shape matching. In SPM 05: *Proceedings of the 2005 ACM symposium on solid and physical modeling.* (pp. 101–106). New York: ACM Press.

Reuter, M., Wolter, F., & Peinecke, N. (2005b). Laplace-Beltrami as shape DNA of surfaces and solids. *Computer Aided Design, 38*, 342–366.

Reuter, M., Wolter, F., Shenton, M., & Niethammer, M. (2009b). Laplace-Beltrami eigenvalues and topological features of eigenfunctions for statistical shape analysis. *Computer Aided Design*, *41*(10), 739–755.

Rhouma, M. B. H., Khabou, M. A., & Hermi, L. (2009). Laplacian and Bilaplacian based features for shape classification. In *Proceeding of the international conference on image processing, computer vision, and pattern recognition.* CSREA Press, Athens.

Ribaric, S., & Fratric, I. (1982). A biometric identification system based on eigenpalm and eigenfinger features. *IEEE Transactions Pattern Analysis Machine Intelligence, 27*, 1698–1709.

Rosin, P. L. (2003). Measuring shape: Ellipticity, rectangularity, and triangularity. *Machine Vision and Applications, 14,* 172–184.

Rumelhart, D. E., Hinton, G. E., & Williams, R. J. (1986). Learning internal representations by error propagation. In D. E. Rumelhart & J. L. McClelland (Eds.), *Parallel Distributed Processing*, Vol. 1. Cambridge, MA: MIT Press.

Saito, N. (2008). Data analysis and representation on a general domain using eigenfunctions of Laplacian. *Applied and Computational Harmonic Analysis, 25,* 68–97.

Sandberg, I. W. (1992). Structure theorems for nonlinear systems. *Multidimensional Systems Signalling Processes, 2,* 267–286, 1991. Errata in 1992, *3,* 101.

Scassellati, B., Slexopoulos, S., & Flickner, M. (1994). Retrieving images by 2D shape: A comparison of computation methods with human perceptual judgments. In *SPIE proceedings on storage and retrieval for image and video databases II,* (Vol. 2185), (pp. 2–14). SPIE (Society of Photo-Optical Instrumentation Engineers), Belligham, WA.

Shah, J. (1998). Segmentation as a Riemannian drum problem. In *Proceedings of the 1998 international conference on image processing*, (pp. 766–769). IEEE, Piscataway, NJ.

Shi, J., & Malik, J. (1997). Normalized cuts and image segmentation. In *IEEE conference on computer vision and pattern recognition.* (pp. 731–737). IEEE, Piscataway, NJ.

Sridhar, S., & Kudrolli, A. (1994). Experiments on not "hearing the shape" of drums. *Physical Review Letters, 72,* 2175–2178.

Stoker, J. J. (1942). Mathematical problems connected with bending and buckling of elastic plates. *Bulletin of the American Mathematical Society, 48,* 247–261.

Strikwerda, J. C. (2004). *Finite difference schemes and partial differential equations* (2nd ed.). Philadelphia, PA: Society for Industrial and Applied Mathematics.

Szegö, G. (1950). On membranes and plates. *Proceedings of the National Academy of Sciences of the United States of America, 36*, 210–216.

Szegö, G. (1954). Inequalities for certain eigenvalues of a membrane of given area. *Journal of Rational Mechanics and Analysis, 3*, 343–356.

Teague, M. R. (1980). Image analysis via the general theory of moments. *Journal of the Optical Society of America, 70*, 920–930.

Torres-Mendez, L. A., Ruiz-Suarez, J. C., Sucar, L. E., & Gomez, G. (2000). Translation, rotation, and scale-invariant object recognition. *IEEE Transactions on Systems, Man, and Cybernetics Part C: Applications and Reviews, 30*(1), 125–130.

Trefethen, L. N., & Betcke, T. (2006). Computed eigenmodes of planar regions. In N. Chernov, Y. Karpeshina, I. W. Knowles, R. T. Lewis, & R. Weikard (Eds.), *Recent advances in differential equations and mathematical physics* (Contemporary Mathematics Vol. 412), (pp. 297–314). Providence, RI: American Mathematical Society.

Turk, R. M., & Pentland, A. (1991). Eigenfaces for recognition. *Journal of Cognitive Neuroscience, 3*, 72–86.

Ullmann, D. (2007). Life and work of E. F. F. Chladni. *European Physical Journal Special Topics: Nodal Patterns in Physics and Mathematics, 145*, 25–32.

Waller, M. D. (1961). *Chladni figures: A study in symmetry.* London: G. Bell.

Wang, Q., & Xia, C. (2010). Universal bounds for eigenvalues of the biharmonic operator. *Journal of Mathematical Analysis and Applications, 364*, 117.

Weinberger, H. F. (1956). Upper and lower bounds for eigenvalues by finite difference methods. *Communications on Pure and Applied Mathematics, 9*, 613–623.

Weinberger, H. F. (1958). Lower bounds for higher eigenvalues by finite difference methods. *Pacific Journal of Mathematics, 8*, 339–368. Erratum, 941.

Weinberger, H. F. (1974). *Variational methods for eigenvalue approximation.* Philadelphia, PA: Society for Industrial and Applied Mathematics.

Weinberger, H. F. (1999). Fichera's method for bounding eigenvalues. *Interactions between analysis and mechanics–the legacy of gaetano fichera.* (pp. 51–65). Atti dei Convegni Lincei 148, Accad. Naz. dei Lincei, Rome.

Weinstein, A. (1937). Etude des spectres des equations aux derivees partielles de la theorie des plaques elastiques. *Membrane Science Mathematical, 88*, 62.

Weinstein, A. (1966). Some numerical results in intermediate problems for eigenvalues. In J. H. Bramble (Ed.), *Numerical solution of partial differential equations* (pp 167–191). New York: Academic Press.

Werbos, P. J. (1974). *Beyond regression: New tools for prediction and analysis in the behavioral sciences*. Doctoral thesis, Harvard University.

Werbos, P. J. (1990). Backpropagation through time: What it does and how to do it. *Proceedings of the IEEE, 78*, 1550–1560.

Weyl, H. (1911). Das asymptotische Verteilungsgesetz der Eigenwerte linearer partieller Differentialgleichungen. *Mathematical Annales, 71*, 441–479.

Wolf, S. A., & Keller, J. B. (1994). Range of the first two eigenvalues of the Laplacian. *Proceedings of the Royal Society of London Series A, 447*, 397–412.

Wu, H., Sprung, D. W. L., & Martorell, J. (1995). Numerical investigation of isospectral cavities built from triangles. *Physical Review E, 51*, 703–708.

Yang, H. C. (1991). An estimate of the difference between consecutive eigenvalues. Preprint IC/91/60 of ICTP, Trieste, 1991.

Yong, I., Walker, J., & Bowie, J. (1974). An analysis technique for biological shape. *Computational Graphics Image Processes, 25*, 357–370.

Zahn, C. T., & Roskies, R. Z. (1972). Fourier descriptors for plane closed curves. *IEEE Transactions on Computational, 3*, 269–281.

Zelditch, S. (2000). Spectral determination of analytic bi-axisymmetric plane domains. *Geometric and Functional Analysis, 10*, 628–677.

Zelditch, S. (2004). Inverse spectral problem for analytic domains. I. Balian-Bloch trace formula. *Communications in Mathematical Physics, 248*, 357–407.

Zelditch, S. (2009). Inverse spectral problem for analytic plane domains II: Z_2-symmetric domains. *Annalen Mathematics and Mathematical, 170*(1), 205–269. Arxiv: math.SP/0111078

Zhang, D. S. (2002). *Image retrieval based on shape*. Doctoral thesis. Australia: Monash University.

Zhang, D., & Lu, G. (2004). Review of shape representation and description techniques. *Pattern Recognition, 37*, 1–19.

Zuliani, M., Kenney, C. S., Bhagavathy, S., & Manjunath, B. S. (2004). Drums and curve descriptors. In T. Ellis & G. Jones. (Electronic Proceedings). *British Machine Vision Conference*, September 2004. London: Kingston University.